Long Wavelength Astrophysics

by

Liam Dean Connor

A thesis submitted in conformity with the requirements
for the degree of Doctor of Philosophy
Graduate Department of Astronomy and Astrophysics
University of Toronto

© Copyright 2016 by Liam Dean Connor

Abstract

Long Wavelength Astrophysics

Liam Dean Connor

Doctor of Philosophy

Graduate Department of Astronomy and Astrophysics

University of Toronto

2016

—

Contents

List of Tables

Chapter 1

Introduction

The most interesting advances in science come not from concerted efforts to answer specific questions, but rather from exploring a new volume of parameter space. The father of observational astronomy, Galileo, did not construct Lippershey's telescope in order to discover the Jovian satellites; instead, he used a novel tool to investigate supra-human magnitudes and spatial resolution to observe three moons "totally invisible by their smallness" orbiting Jupiter (Drake, 1978). The tradition has continued in the centuries since, particularly in astrophysics where we humans have little innate intuition (by definition everything we study is outside of this world). Pulsars, for example, were discovered accidentally with a radio telescope that was built to study interstellar scintillation in quasars (Hewish et al., 1968). The whole field commenced because graduate student Jocelyn Bell noticed extra "scruff" on her chart recorder. Dark matter and dark energy are two more examples of largely unpredicted, but revolutionary, discoveries (Zwicky, 1933; Riess et al., 1998; Perlmutter et al., 1999).

A more recently uncovered phenomenon is the fast radio burst (FRB), a primary focus of this thesis. FRBs were discovered as a result of searching new regions of dispersion measure space at high time resolution. In Sect. 1.1 we will introduce the modern tools that are used to study the long-wavelength sky, and the unprecedented speed and sensitivity

that Moore's law has afforded twenty-first century radio telescopes. After that we will give an overview of some of the science these instruments give us access to, starting with a broad description of the time-variable sky. We will end with an introduction to FRBs in Sect. 1.3 where we outline prominent models and the observations that have informed them.

1.1 Digital telescopes

A telescope's primary purpose is to provide for us spatial, temporal, and chromatic information about electromagnetic fields on the sky. Mathematically, telescopes first perform a spatial Fourier transform (from **x**- to **k**-modes), traditionally with a mirror or reflector, and then another Fourier transform in time (from τ to ν) to separate the signal by wavelength, with, e.g., a diffraction grating. The electromagnetic wave's modulus is typically then squared, destroying phase information, whether with a bolometer or a charge-coupled device (CCD). Modern radio telescopes carry out a similar set of steps, except at some stages they use powerful computers in place analog instrumentation. For example, channelization can be done in software rather than with diffraction. They also have the ability to preserve phase information by measuring a quantity proportional to the electric field, namely voltage.

In an era when electric fields can effectively be sampled billions of times per second, radio telescopes are becoming almost entirely digital. While the cost of constructing large single-dish telescopes is not expected to decrease substantially, the cost of building large computing clusters is, which makes it economically and strategically sensible to point one's telescope and channelize in software. This fact has ushered in a new era of broad-band, wide-field interferometers with large numbers of feeds. These include the Precision Array for Probing the Epoch of Reionization (PAPER), the Murchison Widefield Array (MWA), and the Low-Frequency Array (LOFAR) (Tingay et al., 2013; Parsons et al.,

2014; van Haarlem et al., 2013). The Canadian Hydrogen Intensity Mapping Experiment (CHIME), which is central to this thesis, is another principally digital telescope.

Radio interferometry was first developed in the 1940s when Ryle and Vonberg constructed a dipole array at 175 MHz (Thompson et al., 1986). Based on the Michelson interferometer, it was realized that the same spatial resolution of a large dish with diameter, D, could be achieved by correlating two antennas separated by D. In a classical interferometer, the quantity we measure is called a "visibility", denoted in this text as $V_{m,n}$. It is the time-averaged correlation of the signals, x, between antennas m and n,

$$V_{m,n} = \langle x_m x_n^* \rangle \,. \tag{1.1}$$

This can be written as an integral over all directions, $\hat{\mathbf{k}}$, on the sky, weighted by the complex gains, $g(\hat{\mathbf{k}})$, in that direction.

$$V_{m,n} = \int d^2\hat{\mathbf{k}}\, g_m(\hat{\mathbf{k}})\, g_n^*(\hat{\mathbf{k}})\, T(\hat{\mathbf{k}}) e^{2\pi\, i\, \hat{\mathbf{k}}\cdot\mathbf{d}_{m,n}} \tag{1.2}$$

In Eq. 1.2 the baseline vector between antennas m and n is given by $\mathbf{d}_{m,n}$, and $T(\hat{\mathbf{k}})$ is the sky brightness temperature in the direction $\hat{\mathbf{k}}$. This is not a thermodynamic temperature, but the temperature given by the Rayleigh-Jeans law,

$$T = \frac{c^2\, I_\nu}{2\nu^2\, k_b}, \tag{1.3}$$

where I_ν is specific intensity and k_b is Boltzmann's constant.

For an N-element array, there are $N(N+1)/2$ unique baselines that must be computed, i.e. for each frequency and at each time, Eq. 1.1 must be calculated $N(N+1)/2$ times. Therefore in the large-N limit, the computational cost of the correlation process is $O(N^2)$. Such a scaling means the monetary cost of large interferometers is dominated by computing hardware. One way to get around this is by choosing a highly redundant array, with antennas evenly spaced on a rectangular grid. Instead of correlating all

antennas with one another, the cross-correlation theorem can be employed,

$$\mathscr{F}(\mathbf{x} \star \mathbf{x}^\dagger) = \mathscr{F}(\mathbf{x})\mathscr{F}(\mathbf{x}^\dagger), \tag{1.4}$$

where $\mathbf{x}$ is a vector containing signals from all N antennas. We can therefore calculate the cross-correlation using only spatial Fourier transforms across the array. Inverse Fourier transforming Eq. 1.4, we can reproduce Eq. 1.1 as follows,

$$\left\langle \mathbf{x} \star \mathbf{x}^\dagger \right\rangle = \mathscr{F}^{-1}\left\{\mathscr{F}(\mathbf{x})\mathscr{F}(\mathbf{x}^\dagger)\right\}. \tag{1.5}$$

If the antennas sit on a grid, then the transforms can be computed with Fast Fourier Transforms (FFTs), which scale as $O(N\log(N))$ instead of $O(N^2)$. This was proposed by Peterson et al. (2006) and expanded on in detail by Tegmark & Zaldarriaga (2009). CHIME has such a rectangular array configuration and will be the first large-scale FFT telescope. As we will discuss in Chapters **??** and **??**, the FRB experiment will search 1024 formed beams generated by the algorithm described here.

1.2 The time-domain sky

In the early 1930s Karl Jansky built a steerable 20 MHz antenna in order to locate unaccounted-for receiver noise he had been seeing in transatlantic voice transmissions. He found the signal was periodic in sidereal day and established that the radio emission must be of astronomical origin (Jansky, 1933). In doing so he opened up a new window into the Universe. While astronomers had been observing the sky in the optical for millennia, there was now an wholly new slice of the electromagnetic spectrum with which to view the cosmos.

A similar thing could be said about the time-domain sky. Observing temporal rather than spatial fluctuations gives us access to a swath of new sources, and can help us

better understand the physics of known sources. Pulsars, which proved the existence of neutron stars, could not have been discovered without time-series analysis. The first strong observational evidence for blackholes came from X-ray variations of Cygnus X-1 on timescales of days. A subset of these phenomena vary on human-timescales, but seem not to repeat. We call these transients.

Transients are ephemeral events that can last for milliseconds to months. These include gamma-ray bursts (GRBs), supernovae (SNe), and tidal disruption events. They live in the realm of time-domain astrophysics, but are inherently hard to classify due to their fleeting nature. GRBs, for example, were discovered in the 1960s and are still not well understood. In the radio sky, known transients include flare stars, afterglows from supernovae and GRBs, solar bursts, and now FRBs.

1.2.1 Propagation effects

The two time-varying objects we discuss in this thesis are pulsars and FRBs. Since both live well outside of our solar system and both are observed at long wavelengths, one must consider the various propagation effects that occur in the intervening ionized plasma. In the following subsections we introduce the three most prominent effects. These are dispersion, Faraday rotation, and scattering.

Cold plasma dispersion

Electromagnetic waves traveling through a cold dense plasma will undergo dispersion. Here, "cold" refers to the condition that the thermal velocity of the particles in the plasma is much less than that of the wave, i.e.,

$$v_p \gg v_{ion} = \sqrt{2\,k_B T / m_{ion}}. \tag{1.6}$$

The dispersion results in a frequency-dependent group velocity caused by differential

refractive index in an ionized plasma. The refractive index, n, is given by,

$$n = \left(1 - \frac{\omega_p^2}{\omega^2}\right)^{1/2}, \tag{1.7}$$

where ω_p is the plasma's resonant frequency and ω is the electromagnetic wave's frequency. The plasma frequency is

$$\omega_p = \sqrt{\frac{n_e e^2}{4\pi^2 m\, c}}, \tag{1.8}$$

using e, n_e, and m as the electron charge, number density, and mass respectively. Noting $n = \frac{c}{v_g}$ and plugging this plasma frequency relation into equation 1.7, we can expand about n_e. We get,

$$v_g = c\left(1 - \frac{n_e e^2\, \lambda^2}{2\pi m c^2}\right). \tag{1.9}$$

This equation holds for most of the physics described in this thesis, since the dispersive electron plasmas in the IGM, ISM, and even in the remnants of supernovae are relatively diffuse, with plasma frequencies well below the bands in which we observe. For reference, typical values are $n_e^{IGM} \sim 10^{-7}$ cm^{-3} (Madau, 2000), $n_e^{ISM} \sim 10^{-2}$ cm^{-3} (Lyne & Graham-Smith, 1998) in our Galaxy, and in $n_e^{SNe} \sim 10^{1-3}$ cm^{-3} in remnants (see Chapter 2).

For a single pulse, the light travel-time, t, can be written as the integral, $\int_0^D \mathrm{d}l/v_g$, into which we can plug Eq. 1.9. The frequency-dependent time delay is then,

$$\Delta t = t - \frac{D}{c} \tag{1.10}$$

$$= 1.345 \times 10^{-3}\, \nu^{-2} \int_0^D n_e\, \mathrm{d}l \ \text{ seconds}. \tag{1.11}$$

Here we have switched from angular frequency, ω, to ν in Hz. Dispersion measure (DM) can then be defined as,

$$\mathrm{DM} \equiv \int_0^D n_e \, \mathrm{d}l, \tag{1.12}$$

which is just an electron column density, and is usually reported in units pc cm^{-3}. For a telescope observing between ν_B and ν_T in GHz, the arrival-time difference between the bottom and top of the band will be,

$$\Delta t_{B,T} = 4.15 \times 10^{-3} \, \mathrm{DM} \left(\nu_B^{-2} - \nu_T^{-2} \right) \text{ seconds.} \tag{1.13}$$

While this effect delays all waves with $\nu > \nu_p$, (waves below the plasma frequency will decay exponentially and will not propagate) it is only observationally important for switch sources. Typical pulsars in our Galaxy have DMs between 10-100 pc cm^{-3}, while FRB DMs can be as high as 2000 pc cm^{-3}. The latter gives a dispersion delay of nearly forty seconds between 400 MHz and 800 MHz, where CHIME will observe.

Faraday rotation

If a cold plasma also has a magnetic field, a propagating electromagnetic wave's plane of polarization will be rotated. This is called the "Faraday effect" or "Faraday rotation", named after the nineteenth century English physicist (Faraday & Martin, 1936). The rotation is caused by circular birefringence, meaning left- and right-circularly polarized light travel at slightly different speeds. Since linear polarization can be thought of as the superposition of a right- and left-handed wave, the result is a rotation of the linear polarization vector.

Like dispersion, this effect is chromatic, depending quadratically on wavelength. The linear polarization vector will be rotated by

$$\phi = 2 \, \mathrm{RM} \, \lambda^2 \tag{1.14}$$

where RM is "rotation measure" with units rad m^{-2}. The extent of this rotation depends

on the projection of the magnetic field onto the direction of propagation.

$$\mathrm{RM} = \frac{e^3}{2\pi m^2 c^4} \int_0^L n_e(l) B_\parallel(l) dl \tag{1.15}$$

Here $B_\parallel$ is the component of the magnetic field vector parallel to $\mathrm{d}\vec{l}$. RM can be thought of as an electron-density-weighted mean value of the line-of-site magnetic field between the observer and the source. Conventionally, it is positive for fields directed towards the observer (Manchester & Taylor, 1977).

By dividing Eq. 1.15 by Eq. 1.12 and assuming n_e is roughly constant in whatever medium the radio waves are traversing, one can estimate the average magnetic field in that direction. The ratio of RM to DM is then,

$$\frac{\mathrm{RM}}{\mathrm{DM}} = \frac{e^3}{2\pi m^2 c^4} \frac{\int_0^L n_e(l) B_\parallel(l) dl}{\int_0^L n_e(l) dl} = 0.81 \left\langle B_\parallel \right\rangle \ \mu\mathrm{G}. \tag{1.16}$$

This is a useful tool for understanding the ISM and the structure of the Milky Way's magnetic field.

Scattering

The least understood propagation effect in ionized astrophysical plasma is scattering. Scattered radio waves self-interfere constructively and destructively to produce intensity fluctuations (scintillation), temporal broadening, and angular broadening (Manchester & Taylor, 1977). The cause of this multi-path propagation is still greatly contested (Goldreich & Sridhar, 2006; Pen & Levin, 2014). It was assumed to be due to Kolmogorov turbulence, from which one could easily derive the frequency scalings of temporal scattering ($\tau \propto \nu^{-4}$) and angular broadening ($\theta \propto \nu^{-2}$) (Rickett, 1977). Recently, however, this picture has been called into question by pulsar scintillation observations. Stinebring et al. (2001) found parabolic arclets in Fourier-transformed "dynamic spectra" (a 2D time/frequency field) for a number of pulsars, implying that scattering occurs in just

one or two screens and occurs in localized clumps. Irrespective of the underlying physics, scattering is well-studied phenomenologically. It provides a useful tool not just for studying the ISM, but also for understanding the environment of FRBs. We discuss this both in Sect. 1.3 and Chapter 2.

1.3 Fast Radio Bursts

The discovery of fast radio bursts has captivated the attention of astronomers for two reasons: their origin is a genuine mystery, the likes of which had not been seen in transient astrophysics in decades; and the problem appears to be tractable on timescales of years to a decade. There is good reason to think that with the right survey one could at least determine their radial distribution, as well as the nature of the burst source, if not specific details. This is not true of other major contemporary questions. The tensor-to-scalar ratio, r, in inflationary cosmology, or the deviation of dark energy's w from -1, could be constrained with arbitrary improvements without ever making a detection.

The first FRB was discovered in 2007 by Lorimer et al. (2007a), and has since been called the "Lorimer Burst". Its Galactic latitude ($b = -41.8°$) and large dispersion measure (DM= 375 pc cm^{-3}) implied that the ∼10 millisecond burst was extragalactic (Lorimer et al., 2007a). However, in the years immediately following, no fast transients were seen with DMs exceeding the expected Galactic contribution. This lead to skepticism about the celestial nature of the Lorimer Burst and suspicion that it was terrestrial interference (Burke-Spolaor et al., 2011).

Suspicion that this was a one-off event was relinquished with the discovery of four more FRBs in 2010 in the High Time Resolution Universe (HTRU) survey (Thornton et al., 2013a). Based on the 23 days of observing with a 0.55 deg^2 beam, they reported a surprisingly large rate of $\sim 10^4$ events sky^{-1} day^{-1}. Though their detection made a much stronger case for the extraterrestrial nature of FRBs, it was not unequivocally

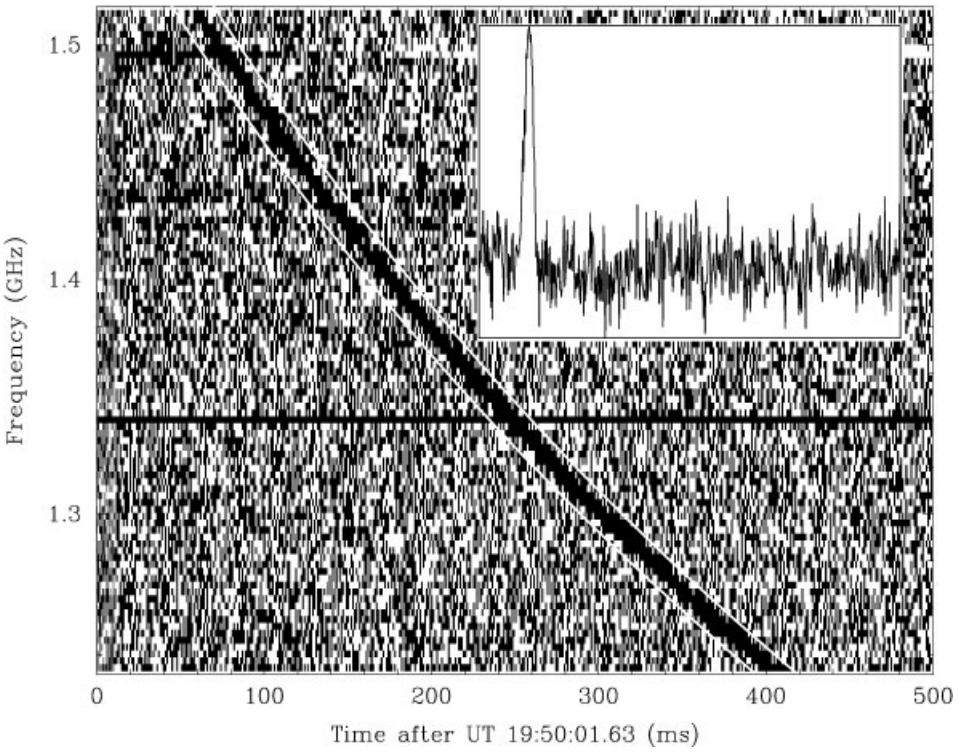

Figure 1.1: Figure reproduced from (Lorimer et al., 2007a) of the so-called Lorimer Burst, which is the first known FRB.

accepted. This is because until the discovery of FRB 121102 in Arecibo's Pulsar ALFA (PALFA) survey, all FRBs had been found with the Parkes radio telescope and in its 13-beam receiver. At Parkes, an unexplained "class" of transients were found in high time resolution data that appeared to be dispersed with hundreds of pc cm^{-3}, and which lasted for ten to a few hundred milliseconds (Burke-Spolaor et al., 2011; Bagchi et al., 2012). These pulses were given the name "Perytons", named after a mythological hybrid animal.

While an astronomical origin for Perytons was excluded early on due to their multi-beam detections, it was not obvious if they were being emitted in the earth's atmosphere naturally, or by something human-made (Katz, 2014; Dodin & Fisch, 2014; Danish Khan,

2014). It was later found by Petroff et al. (2015d) that Perytons were likely caused by an on-site microwave oven. The microwave's magnetron was found to mimic the sweeping λ^2 dependence of truly dispersed sources when the oven's door was opened prematurely (Petroff et al., 2015d). This made sense given the preponderance of events around local noon, i.e. lunchtime.

In the years since Thornton et al. (2013a) discovered their four HTRU bursts, a dozen or so more have been found. These are cataloged online at FRBCAT[1] (Petroff et al., 2016). As we have mentioned, Arecibo's detection of FRB 121102 ensured that the events were not Parkes-specific. Petroff et al. (2015a) found the first FRB in real-time, as well as the first burst for which there was polarization information. FRB 110523 (Masui et al., 2015a) was found in archival data from the Green Bank Telescope (GBT) intensity mapping experiment, which fortuitously saved its data with millisecond time resolution even though it was not strictly necessary for their cosmology. The completed HTRU survey also provided five new sources, found by Champion et al. (2016).

With nearly two dozen detected at the time of this writing, there is still no agreed-upon definition of an FRB. They appear to last for ∼milliseconds, have dispersion measures that are ≥2.5 times that of the Galactic contribution (the range has been $375-1600$ pc cm^{-3}), and maximum flux densities of roughly a Jansky. Exceptions include the Lorimer Burst, which was ∼30 Jy and is the brightest FRB by far, and 010621 whose DM was only about 1.4 times that expected from the Milky Way (Lorimer et al., 2007a; Keane et al., 2012). At both L-band and ∼800 MHz, a detectable rate of several thousand each day over the whole sky now seems likely (Connor et al., 2016a; Champion et al., 2016).

And such ranges are known to be incomplete. Brightness is reported as if the burst were found at the beam's center, so each published flux is a lower limit. We also do not yet know the DM distribution. There may be a population of events with DM $\approx 10^4$

[1] http://www.astronomy.swin.edu.au/pulsar/frbcat/

pc cm^{-3} that are either too rare to see in two dozen bursts, or to which current search algorithms have not been sensitive. Scattering is another poorly constrained parameter. FRBCAT lists five bursts with evidence for scattering, with broadening index around -4, as one would expect (Petroff et al., 2016). However, several sources have been unresolved in time, meaning their width and scattering properties are only constrained from above. The extent and prevalence of scattering is of interest for a couple reasons. One is that it has implications for the source environment, and also because scattering is the limiting factor for low-frequency surveys, like CHIME and LOFAR (Bandura, 2014; van Leeuwen, 2014); an FRB scattered to 10 ms at 1.4 GHz would be several seconds at 400 MHz and effectively undetectable.

1.3.1 Models

Starting with the Lorimer Burst and continuing on to the four high-lat HTRU FRBs, the default assumption was that the progenitors were at cosmological distances (i.e. IGM-induced dispersion). To a lesser extent, the community seemed to assume they did not repeat, in part because of null-result follow up observations that were done (Petroff et al., 2015c), but also because bursts coming from gigaparsec distances might only have enough energy for a single event. It has been argued (Katz, 2016b) that the cosmological interpretation is the most economical way of getting such large column densities of free electrons. In reality, up until recently we did not know their radial distance to better than five orders of magnitude. This is because with such a small sample of events, there was no way of knowing whether they were coming from $z \approx 0.5$, from within our Galaxy, or from our atmosphere.

A significant fraction of this thesis will focus on theoretical elements regarding fast radio bursts. Therefore it would be prudent to provide context for both the history of models that have come in and out of the picture, as well as a time-line of the observations that have informed them. We will start by enumerating the most prevalent theoretical

explanations for the origin of FRBs. They will be lumped into two categories: cataclysmic, in which the progenitor is effectively destroyed, and non-cataclysmic. Note that in Chapter **??** table 2.3 partitions models by their distance and includes each theory's predictions for various observables.

Cataclysmic explanations

- *Blitzars:* Falcke & Rezzolla (2014) suggested that a supramassive neutron star might emit a burst of radio once it has lost its angular momentum and has begun to collapse into a black hole. This collapse will hide the star behind the event horizon and magnetic field lines will snap into place. In this model FRBs do not repeat, since the radio chirp is the object's final signal. The authors also assume these compact objects would be at cosmological distances. Given the known existence of neutron stars with mass greater than the Chandrasekhar limit, Falcke & Rezzolla (2014) conjectured that a few percent of neutron stars are supramassive and rotationally supported, and thereby eventually undergo such a transition. A natural shortcoming of this model is its lack of testable predictions. No electromagnetic counterpart is to be expected, and the proposed gravitational wave counterpart would likely be quite weak.

- *Merging compact objects:* The timescales and energies involved invoke merging compact objects. It has been suggested that NS-NS mergers similar to short-GRBs would satisfy the energetics (Totani, 2013). One might then expect a gamma-ray counterpart. Merging white dwarfs has also been proposed (Kashiyama et al., 2013). It has been suggested that the event rates may not be high enough in these models.

- *Evaporating black holes:* In this model exploding primordial black holes emit energy at wavelengths corresponding to their Schwarzschild radius, which Barrau et al.

(2014) suggest The relation,

$$\lambda_{obs} \propto (1+z)\left(\sinh^{-1}\left[\left(\frac{\Omega_\Lambda}{\Omega_M}\right)^{0.5}(1+z)^{-3/2}\right]\right)^{1/4}, \tag{1.17}$$

gives observable wavelengths of ∼centimeters.

Non-cataclysmic explanations

- *Galactic flare stars:* One of the first non-cosmological, non-cataclysmic models for FRBs suggested they were flaring main-sequence stars in our own Galaxy (Loeb et al., 2014). In this scenario, coronal plasma provides the DM rather than the IGM. The authors argue that the heightened energetics required by FRBs at cosmological distances theoretically motivates nearby sources. The model generically predicts repetition and, of course, overlap with known Galactic variable stars (Loeb et al., 2014; Maoz et al., 2015a).

- *Magnetar flares:* Within one month of publication of the Lorimer event, Popov & Postnov (2007) had proposed that hyper-flares from cosmological magnetars could give rise to highly energetic millisecond bursts. They suggested that an extragalactic soft gamma-ray repeater (SGR) could be generated in a magnetar magnetosphere due to "tearing mode" instability. The emission mechanism of these "millisecond Extragalactic radio burst (mERBS)", as they were - and might have ultimately been - called, was described in 2002 by Lyutikov (2002). The model requires a cosmological population to achieve the large DMs and event rates.

- *Supernova remnant pulsars:* In this model FRBs are very young pulsars, in external but non-cosmological galaxies. Their large dispersion measure from free electrons in their supernova remants, which also Faraday rotates and scatters the burst. The

dispersion measure is given by,

$$\mathrm{DM} \approx \frac{x_e M_{\rm ej}}{m_p \frac{4\pi}{3} v_{\rm ej}^2 t^2} \tag{1.18}$$

, where x_e, $M_{\rm ej}$ are the free electron fraction and supernova ejecta mass respectively, $v_{\rm ej}$, is the ejecta velocity, and t is the age. Proposed by Connor et al. (2016d) as a way of explaining all the observed phenomenology locally, it has been further studied by Piro (2016) and Lyutikov et al. (2016). One firm prediction of this model is that the flux distribution of FRBs will be strictly Euclidean, since their progenitors are in the local Universe ($z \lesssim 0.1$). Further observational consequences of this model, including repetition, are described in 2.

- *Circum-nuclear magnetars:* This model (Pen & Connor, 2015b) infers the existence of radio-loud magnetars at the centers of galaxies from the high-DM (1778 pc cm^{-3}), high-RM (-6.4×10^4 rad m^{-2}) SGR J1745-2900, which is < 1 pc from Sgr A*. Galactic centers would therefore provide the dispersive electron plasma and the bursts would not need to be at cosmological distances, similar to the supernova remnant model. The source of the pulse would be a radio-flare from the nuclear magnetar, similar to the mechanism in (Popov & Postnov, 2007). One issue with this model is the dearth of low-DM FRBs; since radio-loud magnetars exist outside of galactic centers, the model demands that the nuclear sources preferentially emit radio flares.

- *Super-giant pulses:* This is a class of models in which FRBs are akin to giant pulses from the Crab, but several orders of magnitude more energetic. The Crab pulsar, which exhibits the highest known brightness temperatures in the Universe, can get up to ∼MJy. Cordes & Wasserman (2016) provided a detailed investigation into the physical limitations of coherent emission around 1 GHz. Connor et al. (2016d) also use super-giant pulses as the source of the radio bursts. In that model, giant

pulses are necessarily brighter earlier in the young pulsar's life ($\lesssim$ 500 years), which explains why we do not see Crab giant pulses as energetic as an extragalactic FRB. Any version of this model would expect repetition.

1.3.2 Empirical constraints

As of early 2014 no FRB observation presented any standout clues about the emission mechanism. They were all observed only in Stokes I and none had been seen to repeat. With FRB 140514, the first real-time detection, full Stokes information was recorded and immediate follow up observations were carried out in other wavelengths (Petroff et al., 2015b). It was found to have 21±7% circular polarization and negligible linear polarization. No counterpart was found after 12 telescopes from radio to X-ray monitored the FRB field in the days following, ruling out local ($z < 0.3$) SNe and long GRBs (Petroff et al., 2015b).

Between late 2015 and early 2016, there was a rapid succession of significant observational claims. FRB 110523, was the first, published in fall of 2015 (Masui et al., 2015a). It was the only burst after FRB 140514 for which polarimetry could be done. It was found with the GBT IM data in archival data, and had $44 \pm 3\%$ linear polarization (Masui et al., 2015a). Interestingly, the source was Faraday rotated with an RM of -186 rad m^{-2}, which is roughly two orders of magnitude greater than what would be expected in the IGM (Oppermann et al., 2015). This seemed to put strain on the cosmological interpretation of FRB 110523, since the dispersion (caused by free electrons) and the Faraday rotation (caused by free electrons + a magnetic field), would be coming from two different places.

Another exceptional feature of this event was the evidence for two separate scattering screens. Scintillation was found with a ∼MHz decorrelation length as well as temporal broadening at millisecond timescales. The μs scintillation is expected arise when the source enters our Galaxy, implying the ms scattering must happen somewhere local to

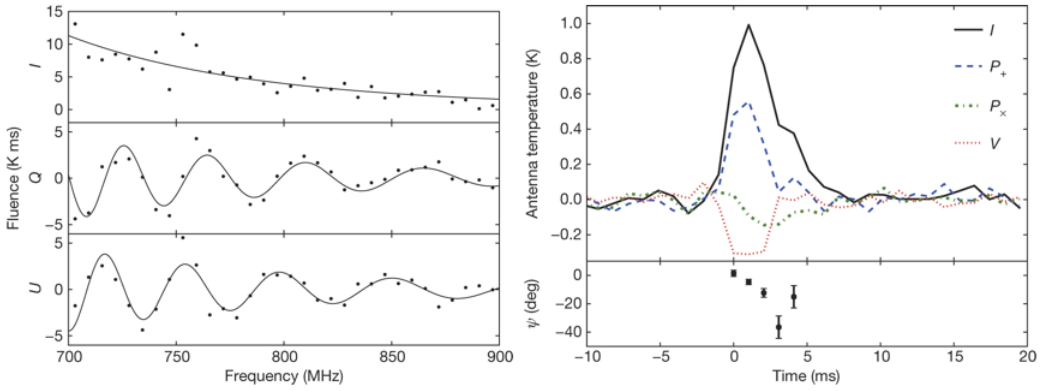

Figure 1.2: Figure adapted from Masui et al. (2015a) of FRB 110523. The left panel shows the large Faraday rotation and the right panel shows the dedispersed, frequency-averaged pulse profiles for total intensity, Stokes V, and the two linear polarizations. One can also see the polarization angle swing across the burst.

the source (Masui et al., 2015a). The FRB also showed a polarization angle swing, similar to that seen in pulsars, indicative of a rotating object. These facts, along with constraints on the dispersing electron's plasma frequencies, ruled out Galactic models. They also lent credence to rotating neutron star models, whether magnetar flares or supergiant pulses from young pulsars.

Another major claim was made by Keane et al. (2016a), who found a host galaxy at $z = 0.492$ that appeared to be associated with an FRB. The localization was not based on a VLBI observation, but rather a coincident radio "afterglow" in the same ∼13" Parkes field. Part of a multi-wavelength follow up, the Australia Telescope Compact Array (ATCA), observing at 5.5 and 7.5 GHz, found a radio source whose flux seemed to fall off a factor of a few in roughly 6 days. The authors interpreted this as a fading

transient, not unlike radio afterglows of short GRBs, favouring the compact object merger scenario. However, the validity of this galaxy's association with the FRB has been called into question. Shortly after the press release of (Keane et al., 2016a), Williams & Berger (2016) did a further observation suggesting the source was in fact a *variable* rather than a transient, the latter of which are quite rare.

By far the most important new observation in the field is the discovery of FRB 121102's repetition (Spitler et al., 2016a). 121102 was found to repeat 10 times in (Spitler et al., 2016a) and 6 additional times in (Scholz et al., 2016a). With one fell swoop the numerous models in the cataclysmic class were falsified. The exception being if there are two or more populations of FRBs with disparate progenitors, in which case "Type A FRBs", for instance, are known to be non-destructive. The sub-bursts were all also detected with Arecibo, many of them getting down to the telescope's fluence limit, implying most of its bursts were undetectable (Spitler et al., 2016a; Scholz et al., 2016a). Its DM changed by less than measurement uncertainty of ~ 6 pc cm^{-3} over the course of several years, though the spectral properties varied wildly from burst to burst. Finally, its repetition was highly non-Poissonian, with 6 of the first 10 appearing in single twenty minute pointing, despite monitoring the field for over ten hours. Such non-Poissonian behaviour was predicted in (Connor et al., 2016b) and has consequences for survey strategy.

1.4 Thesis Outline

In Chapter **??** we introduce the Canadian Hydrogen Intensity Mapping Experiment (CHIME). We start by describing the science goals of the telescope's three back-ends: cosmology, pulsar, and FRB. The instrument is discussed, including a step-by-step outline of the signal chain. This chapter's purpose is to provide context for the other chapters, which either involve CHIME directly or are relevant to its science. Also presented is

early analysis work that I have done, including the discovery of various unexpected beam properties of the CHIME Pathfinder. A simple simulation of aliasing with a 128-feed cylinder is described, which I built. However, since this is a large collaboration, most of the work in this chapter was done by other members of CHIME. For example, the F-engine was built by Kevin Bandura, Jean Francois Trempe, and Matt Dobbs, but it still seemed necessary to describe that step in the data processing. Richard Shaw, Ue-Li Pen, and Kris Sigurdson developed the "m-mode" formalism and pipeline, but it is essential to the science of CHIME cosmology. Details about the instrument in this chapter overlap with the work published in (Bandura, 2014), (Newburgh et al., 2014), and (Berger et al., 2016), all of which I co-authored.

In Chapter **??** we delineate the commissioning of CHIME Pathfinder's beamformer, prefaced by a mathematical introduction to digital beamforming. The work described was done largely by myself, but with the aid of several key people. Andre Recnik was instrumental in networking and miscellaneous computing issues related to the back-end. My supervisor, Keith Vanderlinde was critical in guiding this project in the right direction. The real-time FRB VLBI survey, starting with the burst-search that was attached to the Pathfinder's formed-beam, relied on the direction of Ue-Li Pen and the programming expertize of Kendrick Smith and Kiyo Masui.

Chapter 2 presents a theory for the origin of FRBs in which the bursts are extragalactic but non-cosmological pulsars in the remnants of recent supernovae. We published this model in Monthly Notices of the Royal Astronomical Society (MNRAS) at a time when FRBs were not known to repeat and most authors assumed they were cosmological and cataclysmic (Connor et al., 2016d). This work was done in collaboration with Ue-Li Pen and Jonathan Sievers. It was Jonathan Sievers' idea to place FRBs in young, compact SNe remnants. I then built a model to represent that environment, infer its consequence, and feasibility in terms of event rate and energetics. With Ue-Li I also worked on the observables of the supernova remnant hypothesis as well as other models. These are

included in table 2.3.

Chapter 3 is called "FRB Statistics". In it we analyze a number of statistical problems that have come up since the discovery of FRBs. These include their purportedly non-uniform latitudinal distribution and constraints on their repeat rate. These sections were adapted from a paper published in MNRAS in collaboration with Ue-Li Pen and Niels Oppermann (Connor et al., 2016b). My contribution to this paper included building a model for FRB repetition based on $1/f$ noise and doing mock-follow-up Monte Carlo simulations. Working with Ue-Li, I also developed a test for the latitudinal dependence of the burst-rate that is based on a biased coin flip. This chapter later investigates the all-sky event rate below L-band, and forecasts for CHIME FRB and several other low-frequency experiments. The corresponding sections were derived from (Connor et al., 2016a), again published in MNRAS. As lead author I carried out most of the calculations, excluding the frequentist/Bayesian estimates for event rate, which were conceived of by Niels Oppermann. Hsiu-Hsien Lin and Kiyo Masui, who are members of the GBT IM experiment, provided details about the survey and its dataset. Ue-Li Pen was crucial in the overall direction of the research, particularly in focusing on easily calculable statistics and the idea to forecast by comparing similar surveys. The final paper whose work ended up in Chapter 3 was (Oppermann et al., 2016), accepted to MNRAS. This work was regarding the signal-to-noise distribution of FRBs and the use of a $V/V_{\rm max}$ test. Niels Oppermann created the plots and wrote code to calculate the α/event-rate posterior, but most of the theoretical work was done in meetings with Ue-Li Pen, myself, and Niels.

The final chapter investigates the sub-millisecond structure of individual pulses from B0329+54. The "microstructure" is studied in full polarization, and its quasi-periodicities are found to be common within a pulse for all Stokes parameters, but not common between pulses. This work was done with the supervision of Ue-Li Pen, who provided physical insight and guidance on the project's direction.

Chapter 2

Non-cosmological but Extragalactic Fast Radio Bursts

This chapter was adapted from a paper published in the Monthly Notices of the Royal Astronomical Society called "Non-Cosmological FRBs from Young Supernova Remnant Pulsars" (Connor et al., 2016d). This model explicitly predicts FRB repetition, which had not been observed when the paper was published. We have chosen to leave the language as is, even though it appears out-of-date.

2.1 Introduction

The mystery of fast radio bursts (FRBs) has garnered substantial interest from the radio community. High-energy astrophysicists have tried to model their burst source, observers would like to measure a large population of them, and cosmologists hope to use them as a probe of the intergalactic medium (IGM). However their relative scarcity (only $\sim$ dozen have been observed so far) and their apparent transient nature mean that we still do not know their position on the sky to better than a few arcminutes, and their radial position could be anything from terrestrial to cosmological (Kulkarni et al., 2014).

These objects are highly dispersed, with DMs ($\sim$ 375-1600 pc cm^{-3}) far exceeding

the expected contribution from our own Galaxy's interstellar medium (ISM) (10-100 pc cm^{-3}) and leading to the interpretation that FRBs are cosmological (Lorimer et al., 2007b; Thornton et al., 2013b). Various emission mechanisms have been proposed at a wide range of source locations, including merging white dwarfs (Kashiyama et al., 2013) and neutron stars (Totani, 2013), supergiant pulses from extragalactic neutron stars (Cordes & Wasserman, 2015), blitzars (Falcke & Rezzolla, 2014), magnetars (Popov & Postnov, 2007; Lyubarsky, 2014; Pen & Connor, 2015a), and flaring Galactic stars (Loeb et al., 2014). Though presently there are more theoretical models for FRBs than actual sources discovered, constraints on such theories are rapidly emerging. This is due to recent polarization data, multifrequency coverage, and their being observed by several telescopes at various locations on the sky (Bower et al., 2014; Petroff et al., 2015b).

On top of event rates ($\sim 10^4$ per day per sky) and high DMs, explanations of FRBs must now account for temporal scattering, and the observed polarization states. They should predict or explain Faraday rotation and time-dependent linear polarization. The rotation measure (RM) of our Galaxy has been mapped, and the intergalactic RM is constrained to be less than 7 rad m^{-2} (Oppermann et al., 2015). The observed temporal scattering is problematic for a IGM interpretation, due to the unrealistically small length scales required in the IGM for $\sim$ms scattering (Luan & Goldreich, 2014).

In this chapter we propose a new non-cosmological but extragalactic solution to the FRB problem: supergiant pulses from newly formed pulsars in supernova remnants (SNRs). The dense ionized environment of the SNR can provide 300-2000 pc cm^{-3} of dispersion if the pulses are observed within $\sim$ 100 years of the core-collapse supernova. In our picture the large DM and scattering all come from the same place. The model also generically accounts for substantial Faraday rotation and polarization angle swings. These features were included to account for recent polarization measurements of a new FRB (Masui & Sigurdson, 2015) which may exhibit a polarization vector swing and whose RM is -186 rad m^{-2}. These are not expected in a cosmological interpretation of the DM.

2.2 Supernova Remants

Of order 10^{51} ergs of kinetic energy is released during a supernova, a fraction of which is converted into thermal energy after shock heating of the ejecta plasma. Though the shock-heated ejecta atoms are fully ionized after the explosion, the density is high enough that ionized atoms can soon recombine. This phase of low-ionization comes to an end when the remnant expands into the surrounding ISM, causing a reverse shock wave that reionizes the ejecta. Though this is the basic narrative, observations (Zanardo et al., 2014) as well as simulations (Potter et al., 2014) of SN 1987a have shown that the morphological and ionization properties of SNRs in the decades and centuries after the explosion are nuanced and difficult to model. That said, in general the expanding shell left behind should be able to provide enough free electrons along the line-of-sight for unusually large dispersion measures. If we assume a toy model in which a sphere expands at $v_{\rm ej}$, then the radius R(t) $\approx v_{\rm ej}t$. Therefore the DM we expect can be calculated as,

$$\mathrm{DM} \approx \frac{x_e M_{\rm ej}}{m_p \frac{4\pi}{3} v_{\rm ej}^2 t^2} \tag{2.1}$$

where x_e is the ionization fraction, $M_{\rm ej}$ is the ejecta mass, and m_p is the mass of a proton. Assuming $\sim$10 $M_\odot$ of material is ejected at $v_{\rm ej} \sim 3 - 8 \times 10^3$ km/s and an ionization fraction of $\sim 20\%$, the dispersion measure goes from several thousand pc cm^{-3} immediately after the reverse-shock ionization, to several hundred pc cm^{-3} after 50-100 years (Zanardo et al., 2014). We point out that while the difference between between a sphere of HII, which we have assumed, and a thin shell only slightly alters the DM, it could have a large effect on plasma frequency – something we discuss in section 2.3. In the context of SNR 1987a, Zanardo et al. (2014) found that a possible pulsar could have DMs between 100-6000 pc cm^{-3} after $\sim$ 25 years, though no compact object has yet been observed in that remnant.

Another potentially important feature of the SNR environment is its magnetic field.

The exact magnitude of any detection of Faraday rotation has implications for the possible source location. For instance in the circumnuclear picture, one would expect RMs $\sim 10^{3-5}$ rad m^{-2} (Pen & Connor, 2015a), similar to that of the Milky Way's Galactic center magnetar J1745-29. In the cosmological scenario, if the Faraday rotation came from the same place as the DM - namely the intergalactic medium - then we would only expect a few rad m^{-2} of RM (Oppermann et al., 2015). The Faraday effect rotates the polarization vector by an angle $\phi = \mathrm{RM}\,\lambda^2$, where

$$\mathrm{RM} = \frac{e^3}{2\pi m^2 c^4} \int_0^L n_e(l) B_\parallel(l) dl. \tag{2.2}$$

We can therefore make a rough estimate of the rotation measure of a remnant pulsar with dispersion measure DM. Using Burke & Graham-Smith (2014) we get,

$$\mathrm{RM} \approx 0.81\,\mathrm{rad\,m^{-2}} \times \frac{\langle B_\parallel \rangle}{1\mu\mathrm{G}} \cdot \frac{\mathrm{DM}}{1\mathrm{pc\,cm^{-3}}}. \tag{2.3}$$

Though there is a large uncertainty in evolution of the magnetic field strength and added uncertainty in $\langle B_\parallel \rangle$ given $B_\parallel$ is not necessarily positive, typical values in our Galaxy are 0.2 - 1μG. For instance the Crab and Vela have $\sim 0.92\mu$G and $\sim 0.56\mu$G, respectively. This gives RMs between $\sim 80 - 1200$ rad m^{-2} for a SNR pulsar with FRB-like DMs, which is consistent with (Masui & Sigurdson, 2015).

2.2.1 Event Rates

The daily FRB rate has been estimated at $3.3^{+5.0}_{-2.5} \times 10^3$ sky^{-1} (Rane et al., 2015). If we start from the local core-collapse supernova event rate, Γ_{CC}, and include objects out to some distance $d_{\max}$, we expect the following daily FRB rate,

$$\Gamma_{\mathrm{FRB}} \sim \frac{4}{3}\pi d_{\max}^3 \times \Gamma_{\mathrm{CC}} \times \eta\, \tau_{\mathrm{ion}} \gamma_{\mathrm{GP}} \tag{2.4}$$

where τ_{ion} is the window in years when the SNR is sufficiently dense and ionized to

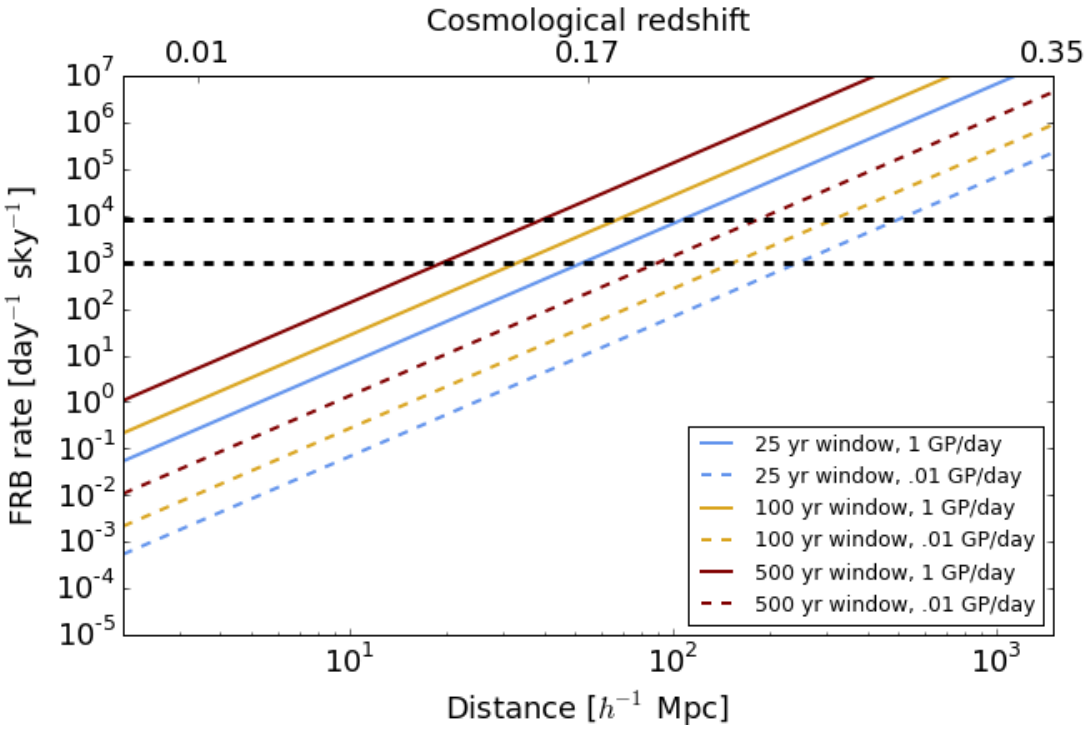

Figure 2.1: Daily FRB rate per sky based on local core-collapse supernova event rate, plotted against distance. We assume early in the pulsar's life there is a window, either 25, 100, or 500 years when the SNR can provide a large enough electron column density to explain the high DMs of the observed bursts. We also include a rate of giant pulses of either one per day or one per hundred days. We have assumed 20% of core-collapse supernovae leave behind a visible pulsar. The horizontal black lines are the 99% confidence bounds for the FRB rate found by Rane et al. (2015).

provide the observed DMs, $\gamma_{\rm GP}$ is the daily rate of giant pulses above $\sim 10^{36}$ ergs, and η is the number of core-collapse supernovae that leave behind a visible pulsar. From Taylor et al. (2014) we know $\Gamma_{\rm CC} \sim 3 \times 10^{-4}$ day^{-1} $(h^{-1}{\rm Mpc})^{-3}$, so if we take $d_{\rm max}$ to be 100 h^{-1}Mpc and $\tau_{\rm ion} \sim 100$ years, we require one giant pulse every 10-20 days, assuming one fifth of this SNe population leaves behind a visible pulsar. In Fig. 2.2.1 we show the event rate as a function of distance, varying two parameters: the effective high-DM window and the rate of giant pulses.

From Fig. 2.2.1 we can see even in our most conservative estimate, when the SNR only has a 25 year window and emits giant pulses once every 100 days, the volume necessary for the highest daily FRB rate is still non-cosmological. By this we mean the

DM contribution from the IGM is less than ~ 200 pc cm^{-3}. If the SNR FRBs are within a hundred h^{-1}Mpc then $\mathrm{DM_{IGM}}$ is less than $\sim 10\%$ of the total dispersion of a typical burst.

If FRBs really are giant pulses then they should repeat stochastically, and while none of the radio follow-ups for observed sources has seen an FRB repeat, this could be because they have not observed for long enough. We point out that FRB 140514, the first burst observed in real-time, was found during a follow up observation of FRB 110220 and the two were found within a beam-width of one another. FRB 140514 had a lower DM than 110220 by 380 cm pc^{-3}, and though Petroff et al. (2015b) show that it was not very unlikely that one would find a new FRB given their integration time, if it were the same source our model could explain the discrepancy. Indeed, a reanalysis by Maoz et al. (2015b) found that the two bursts were far more likely to be the same repeating source than had been previously claimed. Given FRB 110220 would have been emitted over three years earlier, we would expect its DM generically to be higher, but the amount would depend on the inner structure of the SNR and its expansion speed. We discuss repetition further in section 2.3.

2.2.2 Young SNR Pulsars

About a dozen pulsars in our Galaxy are known to emit extremely energetic, short duration radio pulses which can be many orders of magnitude brighter than the pulsar's regular emission. Some of these objects exhibit a rare tail of *supergiant* pulses, whose brightness temperatures exceed the Planck temperature, $\gtrsim 10^{32}$ K (Cordes et al., 2004), which we will take as a working definition of *supergiant*. Indeed the largest known brightness temperature, T_b, in the universe came from a giant pulse from the Crab, with $T_b \sim 2 \times 10^{41}$ K (Taylor et al., 2014). Though there are only ~ 100 hours of published giant pulse data from the Crab, it is known that the supergiant pulse tail does not obey the standard power-law fall off in amplitude (Mickaliger et al., 2012).

Given the relatively high frequency of core-collapse supernovae in the local universe, the young rapidly rotating pulsars such events leave behind could emit giant pulses bright enough to be observed at hundreds of megaparsecs. These supergiant pulses would require 10^{36-37} ergs of output, assuming and observed flux density of 0.3-5 Jy and $\sim$ 500 MHz of bandwidth over 1 ms. Though this is $\sim$ billions of times brighter than an average pulse, it is negligible compared to a pulsar's total rotational energy, $E_{rot} \sim 10^{49-50}$ ergs, and even the pulsar's spin-down luminosity. We also point out that given its relative proximity, this model requires a couple orders of magnitude less energy than cosmological FRBs, located beyond a Gpc.

The polarization properties of giant pulses are also consistent with those of observed FRBs. Giant pulses are known to be highly polarized, switching between strong Stokes V and purely linearly polarized states often in an unpredictable way. The only published FRB prior to Masui & Sigurdson (2015) with full-pol information was FRB 140514 and was found to have $\sim$ 20% circular polarization and no detectable linear polarization (Petroff et al., 2015b). If FRBs were coming from a pulsar-like emission mechanism, one might see nearly pure Stokes V or linear-pol states. Another consequence of pulsar-like emission is that FRBs could exhibit polarization angle swings over the burst duration, which was observed by Masui & Sigurdson (2015). Unfortunately, to date all other published FRBs were detected with systems that recorded only Stokes I.

2.3 Predictions

In table 1 we summarize the observational consequences of ours and several other models as best we can. As one might expect, the most striking differences in predictions has to do with the distance of FRBs, for example the cosmological FRB models differ from each other mainly in their expected counterpart and not much else.

The young SNR pulsar model makes several predictions that will be addressed with

Location	**Model**	**Galactic scintillation**	**Faraday rotation**	$\frac{\mathbf{dlnN_{FRB}}}{\mathbf{dlnS_\nu}}$	**Counterpart**	**DM range (pc cm^{-3})**	**Pol angle swing**
Cosmological ($\gtrsim 1h^{-1}$Gpc)	Blitzars	×	$\lesssim 7$ rad m^{-2}	?	gravitational waves	300-2500	×
	Merging COs	×	$\lesssim 7$ rad m^{-2}	?	type Ia SNe, X-ray, γ-ray	300-2500	×
	Primordial BHs	×	$\lesssim 7$ rad m^{-2}	?	$\sim$TeV	300-2500	×
	Magnetar flare	×	$\lesssim 7$ rad m^{-2}	?	$\sim$ms TeV burst	300-2500	✓
Extragalactic, local ($\lesssim 200h^{-1}$Mpc)	Edge-on disk	✓	50-500 rad m^{-2}	-3/2	?	10-2000	?
	Nuclear magnetar	✓	10^{3-5} rad m^{-2}	-3/2	none	10-3000	✓
	SNR pulsar	✓	20-10^3 rad m^{-2}	-3/2	archival CC SNe or nearby galaxy	10^2-10^4	✓
Galactic ($\lesssim 100$ kpc)	flaring MS stars	✓	$\mathrm{RM_{gal}}$	-3/2	main sequence star	$\gtrsim 300$	×
Terrestrial ($\lesssim 10^5$ km)	RFI	×	$\lesssim \mathrm{RM_{ion}}$	$\begin{cases} -1/2\ if\ 2D \\ -3/2\ if\ 3D \end{cases}$	none	?	×

Table 2.1: This table summarizes a number of FRB models by classifying them as cosmological, extragalactic but non-cosmological, Galactic, and terrestrial. The seven columns are potential observables of FRBs and each row gives their consequence for a given model (Blitzars (Falcke & Rezzolla, 2014), compact object mergers (Mickaliger et al., 2012; Totani, 2013), exploding primordial blackholes (Barrau et al., 2014), bursts from magnetars (Lyubarsky, 2014), edge-on disk galaxies (Xu & Han, 2015), circumnuclear magnetars (Pen & Connor, 2015a), supernova remnant pulsars, stellar flares (Loeb et al., 2014), and terrestrial RFI (Hippke et al., 2015).). For the latter, we subdivide the RFI into planar RFI (2D) coming from the earth's surface, and 3D RFI coming from objects like satellites. Since scintillation only affects unresolved images, cosmological sources that are not scattered near the source will not scintillate in our Galaxy, while non-cosmological sources whose screens are intrinsic will. For Faraday rotation and scintillation we assume the RM and SM comes from the same place as the DM, e.g. the IGM for cosmological sources, though such models could introduce a more local Faraday effect or a scattering screen. Even though all models have to explain the observed 375-1600 pc cm^{-3}, some models predict a wider range of DM. For instance, in the circumnuclear magnetar or edge-on disk disk scenarios there ought to be bursts at relatively low DM that simply have not been identified as FRBs. In our supernova remnant model DMs should be very large early in the pulsar's life, though this window is short and therefore such high DM bursts would be rare.

more data, particularly with full polarization observations and large field-of-view surveys. The latter will provide a large sample of FRBs whose flux and DM statistics can give us information about their location. Since in the SNR FRB picture most of the DM is intrinsic, the sources do not need to be at cosmological distances. This means the flux distribution is given by a Euclidean universe that is only weakly dependent on DM, $N(>S) \propto S^{-3/2}$. Wide-field surveys like CHIME (Bandura, 2014) (whose FRB back-end will observe steadily for several years), UTMOST[1], or HIRAX could observe as many as $\sim 10^{3-4}$ per year, which would allow for detailed population statistics. An instrument like CHIME will not only give us large numbers of DMs and fluxes, but will also allow us to measure various polarization properties and frequency scintillation.

Since we have proposed that FRBs come from young pulsars in SNRs, it is possible that the corresponding supernova was observed in recent decades in the optical. If the pulsars were younger than ∼60 years old they could be localized at the ∼arcsecond level and matched against catalogued type II supernovae, though we would need a large sample of FRBs given the incompleteness of recorded supernovae. With current data the location of FRBs has been too poorly constrained to say anything meaningful about overlap with historic SNe or coincident galaxies; out to ∼150 h^{-1}Mpc there are a number of galaxies in a Parkes beam and therefore one would expect as many supernovae anyway in the last century, even though it would not likely have been observed. However better localization or a cross-correlation between a large sample of FRBs and nearby galaxies could help support the non-cosmological extragalactic FRB hypothesis.

We also point out that while FRBs seem not to repeat regularly, it is not known that they never repeat. Though the statistics of giant pulses from local pulsars are mostly Poisson (Sallmen et al., 1999), it is possible that the supergiant pulses we require from very young SNR pulsars are not. If their statistics were of a Poisson process then there are already limits on the repeat rate, given the $\sim$ 100 hours of follow up, however if their

[1]http://www.caastro.org/news/2014-utmost

statistics were more like earthquakes, the brightest pulses could burst intermittently and turn off for extended periods. It is possible that FRBs could repeat every 5-500 days. If they were to repeat, it is possible that their DMs, RMs, and scattering properties could change noticeably on months/years timescales. Unlike standard pulsars whose RMs and DMs are constant to a couple decimal places, young SNR pulsars like the Crab and Vela have shown significant - and sometimes correlated - variation in such properties (Rankin et al., 1988). As discussed in section 2.2.1, FRB 140514 had a DM that was several hundred pc cm^{-3} smaller than FRB 110220 and the two were found within a beam-width of one another. Though this could have just been a spatial coincidence of two separate objects, our SNR FRB model could account for such a change in DM while other models (cosmological, edge-on galaxy, etc.) cannot.

We also predict that such repeated bursts could have vastly different polarization states, similar to the giant pulses from pulsars in the Galaxy. Another consequence of polarized pulsar-like emission would be a polarization angle swing. Given the FRBs would be rotating, the angle of the linear polarization vector could change throughout the pulse – a phenomenon that is seen in many galactic pulsars, often repeatably (Becker et al., 2006). Therefore models that explain FRBs as rapidly rotating compact objects could predict a swing in the polarization angle throughout the burst.

Depending on the relationship between the giant pulse rate and SNR age and environment, there may exist a short window in the pulsar's life when DMs are larger than could be achieved in the IGM at redshifts $z \lesssim 2.5$. Naïvely we would expect the average pulse energy to decay with time along with its period. It would be therefore possible, albeit rare, that an FRB have a DM of $\sim 10^4$ pc cm^{-3}. In general we expect the distribution of DMs to be peaked somewhere around the observed FRBs (500-800 pc cm^{-3}), but with weight at intermediate DMs when the ejecta has significantly expanded and at very high DMs. In several non-cosmological FRB models there should be a number of low-DM FRBs (Pen & Connor, 2015a; Xu & Han, 2015), which must be explained

away with non-identification bias. However in our picture we do not expect the pulsar to emit supergiant pulses indefinitely and therefore we do not expect to be able to see these objects when the SNR has expanded and the DMs would be moderate. In the Katz (2016c) treatment of the SNR FRB it is assumed that the supergiant pulse rate is time-independent, a scenario that the observed $\frac{\mathrm{d}\log N}{\mathrm{d}\log DM}$ has already cast doubt on. But since the DM distribution depends on birth spin rate and the dependence of luminosity with period, both of which are unknown, we do not attempt to predict it concretely. The Crab would need to emit giant pulses in excess of several GJy to be seen at the distances we are proposing - which is several orders of magnitude brighter than what has been observed - and we postulate that is does not because it is too old.

Beyond the varying DM distributions produced by the location, density, and time dependence of the dispersing electrons, their plasma frequency can give interesting constraints on the nature of FRBs. Since

$$\omega_p = \sqrt{\frac{n_e e^2}{m_e \epsilon_o}} \tag{2.5}$$

we expect FRBs dispersed by the diffuse IGM to have very low plasma frequencies while Galactic models, e.g. flaring stars, should predict large ω_p. This can be verified in in precise measurements of the pulse arrival time as a function of frequency. If $k^2c^2 = \omega^2 - \omega_p^2$, then the λ^2 arrival time dependence is only true in the limit where $\omega >> \omega_p$. Therefore plasma frequency can be used to test FRB models by looking for deviations in the data. This probe was also pointed out by Katz (2016c), who shows the dispersion index for $\Delta t \propto \nu^\alpha$ differs from -2 by $\frac{6\pi n_e e^2}{m_e \omega^2}$. In the SNR model a ∼50 year SNR expanding at $\sim$ 3,000 km s^{-1} would have a plasma frequency of $\lesssim$ 10 MHz and an arrival delay within 4×10^{-5} of -2.0 at 1.4 GHz, which is consistent with present measurements.

Another interesting path for studying extragalactic radio bursts, cosmological or otherwise, is scintillation. Only objects of small angular size scintillate, which is why stars twinkle and planets do not: turbulent cells in the ionosphere can resolve planets but not

stars. The same is true for extragalactic objects scintillating in the Milky Way, where objects larger than $\sim 10^{-7}$ arc seconds do not scintillate at ∼GHz. This is why so few quasars scintillate (Dennett-Thorpe & de Bruyn, 2002).

While several explanations for this scintillation exist (Narayan, 1992; Pen & Levin, 2014), we are concerned with the observational effects and not the physics. Using Thompson et al. (1986) we can estimate the angular size of an extragalactic object,

$$\theta \approx \left(\frac{2c\tau \left(R_{\rm obj} - R_{\rm sn} \right)}{R_{\rm sn} R_{\rm obj}} \right)^{1/2} \tag{2.6}$$

where $R_{\rm obj}$ is the distance to the source, $R_{\rm sn}$ is the distance to the screen, and τ is the scattering timescale. For the case of FRBs we take τ to be ~ 10 ms. In the cosmological case, if the ms scattering were from an extended galactic disk along the line of sight (see McQuinn (2014)) halfway between us and the source, then the angular broadening of an object at 2 Gpc is ~ 150 microarcseconds. If the screen were within 1 kpc of the same object then the broadening is ~ 80 nanoarcseconds. Therefore scintillation from our own Galaxy should only occur for cosmological FRBs whose millisecond scattering is close to the source. For an SNR FRB the screen would have to be within a few hundred parsecs of the object, which we generically expect. We include this feature in table 1 where each column is estimated based on the medium that is causing the high dispersion measure, e.g. the IGM for cosmological models.

2.4 Conclusions

Evidence is emerging suggesting FRBs are not only extraterrestrial but extragalactic. Though the simplest interpretation of their high DMs is a cosmological one, we find this model less compelling in the light of past scattering measurements and potential Faraday rotation and pol-angle swing in a new FRB (Masui & Sigurdson, 2015). In this chapter we offered a more nearby solution. We have gone through a model in which FRBs are

really supergiant pulses from extragalactic supernova remnant pulsars, within a couple hundred megaparsecs. The SNR environment is sufficiently dense and ionized to provide DMs $\gtrsim$ 500pc cm^{-3} as well as RMs $\gtrsim$ 50 rad m^{-2}, only the first of which could be replicated by the IGM.

The environment could also provide $\sim$ms scattering at 1 GHz, as has been observed in Galactic SNR pulsars. That makes this picture self-contained in the sense that the young remnant environment can account for the dispersion and scattering measure seen in FRBs. It predicts a higher Faraday rotation than the IGM, but not as high as galactic centers. The repetition rate is related to the distance, and could be from days to years. By extrapolating Crab-like giant pulses back to the pulsar's first century or so, we have proposed that such objects can emit extremely energetic bursts sporadically. If these are similar to giant pulses from Galactic pulsars, they could be highly polarized, either linearly or circularly, and if they were to repeat their polarization state may change drastically. Given the object's rotating nature, polarization angles would be likely to swing during the pulse. The distinct polarization properties have been seen in at least one burst and may be end up being generic properties of FRBs (Masui & Sigurdson, 2015).

2.5 Acknowledgements

We thank NSERC for support. We also thank Bryan Gaensler, Niels Oppermann, Giovanna Zanardo, and Chris Matzner for helpful discussions.

Chapter 3

Fast Radio Burst Statistics

This chapter was adapted from three separate papers published in the Monthly Notices of the Royal Astronomical Society that explored the statistics of FRBs. In (Connor et al., 2016b), or "FRB repetition and non-Poissonian statistics", it was argued that FRBs may repeat with unusual statistics. Connor et al. (2016a), or "Constraints on the FRB rate at 700-900 MHz", provided detailed constraints on the FRB rate below L-band, and in "The Euclidean distribution of Fast Radio Bursts" we discussed the best way of calculating $N(> S)$ (Oppermann et al., 2016). Due to the rapid progress in this field over the last several years, these papers straddle major discoveries. For example, when (Connor et al., 2016b) was put on the ArXiv, (Spitler et al., 2016b) had not yet been published and FRBs were not known to repeat.

3.1 Chapter Overview

In this chapter we discuss a number of statistical issues related to FRBs. Although the Lorimer burst was discovered in 2007, in 2013 there were still fewer than half a dozen detected events. That meant inference about the nature of FRBs based on their statistics was difficult, and early statistical claims seemed to us to over-reach. For example, Petroff et al. (2014) claimed that the absence of events in the lower-latitude components of

the High Time Resolution Universe Survey (HTRU) compared to the higher-latitude region was significant at the level of 99.5%, based on four FRBs the high-lat region. Furthermore, this dearth at low latitudes was reportedly significant enough to require something beyond heightened scattering and effective system temperature in the Galactic plane. This prompted explanations for why there might be so many more off the plane than near it (Macquart & Johnston, 2015). However, we found the discrepancy to be less severe by a factor of a few, and that even with five more events in the high-lat component of HTRU the p-value is only about 5%. This work is discussed in Sect. 3.4, as adapted from (Connor et al., 2016b).

We have also attempted to urge the community not to jump the gun on the nature and location of FRBs. Before FRB 121102, by far the most popular class of explanations for FRBs was the cosmological cataclysmic one. This is the scenario in which the IGM accounts for nearly all of the burst's DM, and the pulse is caused by a one-off event, like merging compact objects. Keane et al. (2016a), for example, carried out a multi-frequency follow-up of FRB 150418. They interpreted diminishing radio emission from a galaxy at $z \approx 0.5$ as an FRB host galaxy and afterglow from coalescing neutron stars after observing a burst in that direction. This claimed was later questioned by Williams & Berger (2016), who suggested this was AGN variability, and not a transient. Before the discovery of FRB 121102's repeat bursts, we suggested that the limits on repetition might be weakened if they repeated with non-Poissonian statistics, and that the repeating scenario ought not be ruled out (Connor et al., 2016d,b). 121102 was found not only to repeat 16 times, but to do so in a highly non-Poissonian way. The events seem to be closely clustered in time, such that even though the average repeat rate is roughly once per hour, it is not unexpected to go $\sim$12 hours without seeing one. We discuss this work in Sect. 3.2.

Calculating and discussing the event rate of FRBs requires some statistical care. In Sect. 3.3 we make the first estimate of the burst rate below 1.4 GHz. We also discuss the

problems related to quoting an all-sky rate above a strict fluence threshold, and instead offer a more direct method of predicting a rate for a given telescope. This work was first published in (Connor et al., 2016a).

Another statistical approach to probing the location of fast radio bursts is to use their flux distribution $N(> S)$. We find in Sect. 3.5 that given the detected events at the time of this writing, the distribution of FRBs is consistent with a Euclidean one. A recent paper (Vedantham et al., 2016) has attempted to model the Parkes beam in order to infer information about the true brightness of bursts it has seen, and we will discuss this briefly in the conclusions.

3.2 Rethinking the constraints on repetition

Though no source has been shown with certainty to repeat, the limits on repeatability of FRBs are still weak. Several models generically predict repetition, whether periodic or stochastic. Galactic flaring stars (Maoz et al., 2015a), radio-bursting magnetars (Popov & Postnov, 2007; Pen & Connor, 2015a), and pulsar planet systems (Mottez & Zarka, 2014) all predict repetition with varying rates and burst distributions.

In Connor et al. (2016d) it was suggested that supergiant pulses from very young pulsars in supernova remnants of nearby galaxies could explain the high DMs, Faraday rotation, scintillation, and polarization properties of the observed FRBs. We proposed that if the repetition of supergiant pulses were non-Poissonian (with a pink or red distribution) then one might expect several bursts in a short period of time. It is also worth mentioning that the statistics and repeat rates of FRBs could vary from source to source – even if they come from a single class of progenitors – so a long follow-up on an individual burst may not provide global constraints. In this chapter we will refer to stationary Poisson processes (expectation value, $\mu(t)$, is constant in time) as "Poissonian". When we discuss non-Poissonian statistics we will be focusing on stochastic processes that are

correlated on varying timescales. For example we will not discuss periodic signals, which are not Poissonian but have already been studied (Petroff et al., 2015c).

3.2.1 Flicker noise

Pink noise is ubiquitous in physical systems, showing up in geology and meteorology, a number of astrophysical sources including quasars and the sun, human biology, nearly all electronic devices, finance, and even music and speech (Press, 1978; Voss & Clarke, 1975). Though there is no agreed-upon mathematical explanation for this phenomenon (Milotti, 2002), fluctuations are empirically known to be inversely proportional to frequency for a variety of dynamical systems. This can be written as

$$S(f) = \frac{C}{f^{\gamma}} \quad \text{if} \quad f_{\min} \leq f \leq f_{\max}, \tag{3.1}$$

where $S(f)$ is the spectral density (i.e. power spectrum), γ is typically between 0.5-2, and $f_{\min}$ and $f_{\max}$ are frequency cutoffs beyond which the power law does not hold. In this chapter we will describe these distributions as having flicker noise.

In the case of a time-domain astronomical source, this results in uniformity on short timescales, i.e. a burst of clustered events followed by extended periods of quiescence. If FRBs were to exhibit such flicker noise then their repetition would not only be non-periodic, but would also have a time-varying pulse rate and, more importantly, variance. Therefore the number of events seen in a follow-up observation would depend strongly on the time passed since the initial event.

In Petroff et al. (2015c) the fields of eight FRBs discovered between 2009 and 2013 were followed up from April to October of 2014, for an average of 11.4 hours per field. During this follow-up programme FRB 140514 was found in the same beam as FRB 110220, however the authors argue that it is likely a new source due to its lower DM. After its discovery, the field of 140514 was monitored five more times, starting 41 days

later on 2014-06-24, without seeing anything. Under the assumption that 140514 was a new FRB that only showed up in the same field coincidentally and that the repeat rate is constant, Petroff et al. (2015c) rule out repetition with a period $P \leq 8.6$ hours and reject $8.6 < P < 21$ hours with 90% confidence. However it is possible that one or both of those premises is invalid, so it is useful to explore the possibility of non-stationary repeat rate statistics and repeating FRBs with variable DM.

If the statistics of the FRB's repeat rate were non-Poissonian and initial bursts from FRBs were to have aftershocks similar to earthquakes, then the non-immediate follow-up observations impose far weaker repeat rate limits than has been suggested. We constructed a mock follow-up observation of the eight FRBs whose fields were observed in Petroff et al. (2015c). We then asked how many bursts are seen to repeat if we do an immediate follow-up vs. a follow-up several years after the initial event at times corresponding to the actual observations carried out.

We run a simple Monte Carlo simulation with one sample per hour and a probability of 0.5 that a given sample has a burst in it. The repeat rate of once per two hours is chosen arbitrarily and should not affect the comparison. To get the $1/f^{\gamma}$ distribution we take an uncorrelated Gaussian time stream centred on 0 and move to Fourier space, then multiply by $f^{\gamma/2}$, which gives a power spectrum with the desired shape. We then inverse Fourier transform back to get the pink or red time stream. We then take samples with a positive value to contain a pulse and samples with a negative value to contain none.. In the stationary Poisson case, the rate of bursts in the immediate follow-up is the same as the multi-year follow-up since all times are statistically equivalent. However with flicker noise the variance is strongly time-dependent. If we imagine an object that repeated on average once per two hours, then if those pulses were Poisson-distributed the probability of seeing zero bursts in 11.4 hours or longer is $\sim$0.007. With pink noise one expects this roughly 20% of the time, since the system prefers either to be in "on" or "off" mode. If the average repeat period were more like 5-20 hours, then we would often see nothing in

a multi-day follow-up observation that took place weeks or years after the initial event.

This is consistent with what Petroff et al. (2015c) saw, though the conclusions differ depending on the assumed statistics. In Fig. 3.1 we show a sample from this simulation for three repeat distributions. The right panel shows how, if an FRB's burst rate has long-term correlations ($1/f^{\gamma}$), the likelihood of a repeat is greatly increased if the follow-up observation is immediately after the initial event, rather than months or years after.

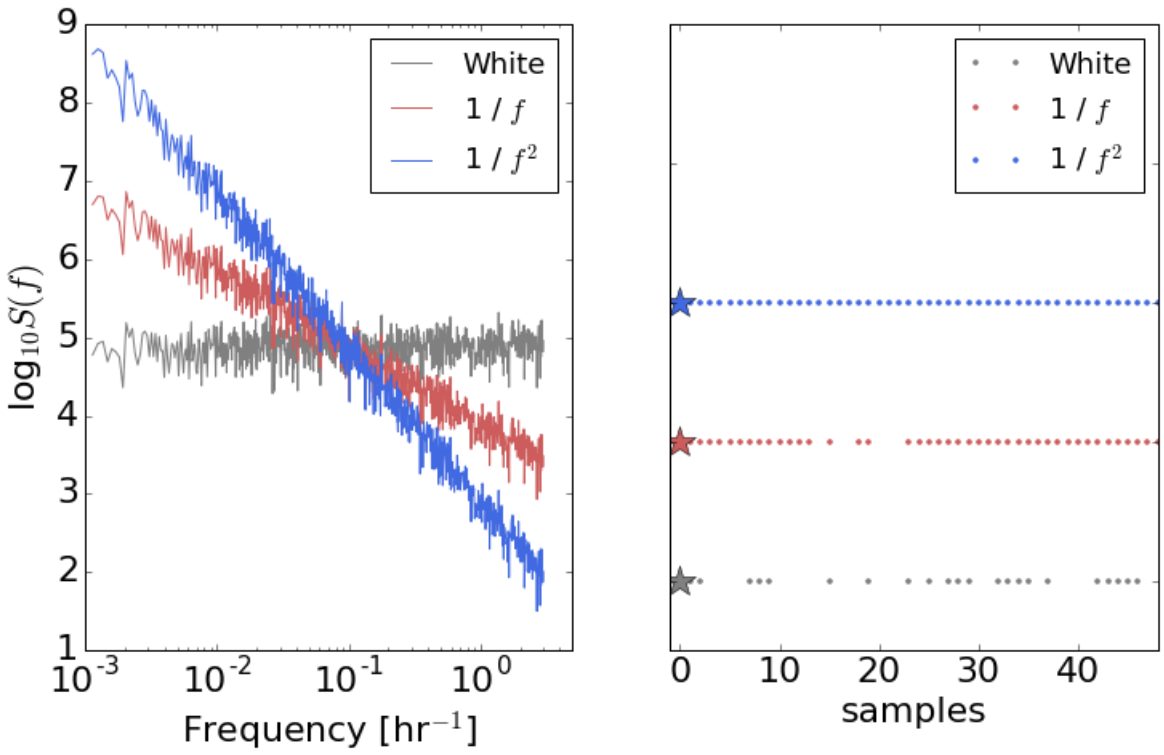

Figure 3.1: Realization of our mock follow-up Monte Carlo. *Left panel*: Power spectrum for pulse arrival times of a single FRB. Grey shows a flat spectrum, corresponding to the often assumed Poissonian repetition rate. The red and blue spectra show flicker noise, with pink ($1/f$) noise and Brownian ($1/f^2$) noise respectively. *Right panel*: We found the first "event" in our Monte Carlo (represented by a star) for the three different spectra and plotted their behaviour in the subsequent 48 hours of follow-up. Though the average probability over the whole simulation is 0.5 for each distribution, when we zoom in on this short period the strong time-like correlations in the $1/f^{\gamma}$ cases means there are many repetitions: they are in an "on" state at this time.

3.2.2 FRBs 110220 and 140514

Using the event rate of roughly 10^4 sky^{-1} day^{-1} from Thornton et al. (2013b), it was originally reported that the probability of seeing a new FRB in the field of 110220 during the 85 hours of follow-up was 0.32 (Petroff et al., 2015b). It was then pointed out by Maoz et al. (2015a) that this underestimated the coincidence by an order of magnitude, since they estimated the rate in any one of the 13 beams, while the new event occurred in the identical beam. The probability also dropped due to the updated daily event rate, given the Thornton et al. (2013b) estimate is now thought likely to be too high. In general we expect the true rate of FRBs to be lower than what is reported due to non-publication bias: If archival data are searched and nothing is found, it is less likely to be published than if something is found. That said, using the rate calculated by Rane et al. (2016) and following the procedure of Maoz et al. (2015a), we find the likelihood of finding a new burst to be between 0.25-2.5%.

Given the relatively low probability of finding a new FRB in the same field and since there are models that predict burst repetition with variable DMs (Connor et al., 2016d; Maoz et al., 2015a) one can ask the question: If one FRB out of eight is found to repeat during 110 hours of follow-up (including extra time spent on 140514), what are the limits on the average repeat period? Another way of asking this question is what is the probability of some number of repetitions during the 110 hours, given a repeat rate. The answer to this question depends strongly on the power spectrum's shape. For the sake of example, if the average repeat rate is once per two hours, then the probability of one repeat or fewer in the Poisson case is effectively zero. With a pink distribution it is closer to 5%, even though the expected number would be 55. This is shown in Fig. 3.2, in which we plot the probability of seeing zero or one repeat burst (the two options for FRB 140514), given some average repetition period, P. We generate the pink distribution in the same way described in Sect. 3.2.1, using one-hour samples and a long-wavelength cutoff at 1.2 million hours. Though it was taken arbitrarily, the probability

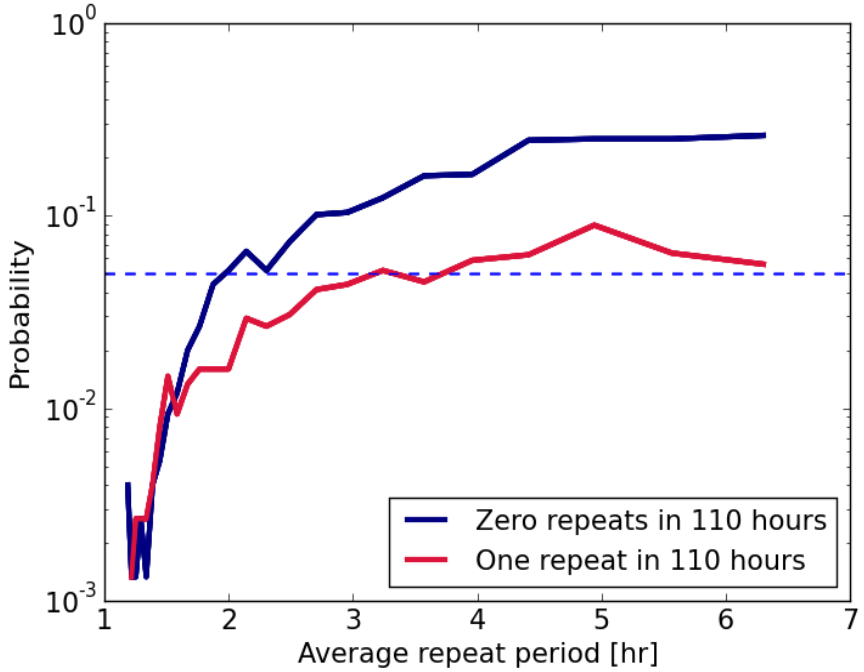

Figure 3.2: The probability of seeing zero (blue curve) or one (red curve) repeat burst in 110 hours of follow-up, assuming a $1/f$ distribution. The curves are derived from a simple Monte Carlo in which a pink distribution was generated with one sample per hour, and we asked how many bursts were seen in 110 samples. Thousands of 110-hour realizations were then averaged for each repeat period, P. Even with an average repeat rate of once every two hours, there is still a 5% chance (indicated by the dashed line) of seeing one or fewer bursts, despite the expected value of 55.

of seeing no bursts should depend only weakly on this cutoff. Since the variance scales logarithmically with this number, there is only roughly a factor of three difference in total power between our choice and $f_{\rm min} \sim$ an inverse Hubble time. While we remain agnostic about the relationship between 140514 and 110220, with non-Poissonian repetition it is possible to have a relatively high repeat rate and to see either one or zero repeat bursts in several days of observation.

3.2.3 Repetition and total number of sources

If FRBs were found to repeat, their statistics and the average frequency of their repetition should affect the search strategy of upcoming surveys. For instance, if it were found that

FRBs repeated, on average, five times a day, then the number of unique sources would be five times smaller than the per-sky daily event rate. This means the daily rate $3.3^{+5.0}_{-2.5}\times10^3$ sky^{-1} estimated by Rane et al. (2016) would be produced by only ∼160-1600 sources. In this scenario there is no FRB in most pixels on the sky, which means one could integrate on most patches forever without seeing an event. An example of this strategy is the VLA millisecond search, in which ∼40% of the time was spent at a single pointing, and almost three quarters of the time was spent at just three locations (Law et al., 2015). It is possible that pointing-to-pointing event rate variance contributed to their not seeing anything.

We therefore warn that deep surveys are at a disadvantage to those that sweep large regions of the sky (CHIME (Bandura, 2014), UTMOST[1], HIRAX) because the non-repeating scenario is unaffected; whereas shallow observations should not hurt the detection rate, no matter what their repetition. Ideally, a survey needs only to spend a few dispersion delay times on each beam before moving on.

3.3 FRB 110523 and sub-L-band statistics

To date, estimating the all-sky rate of FRBs has proven difficult, even at 1.4 GHz where most have been found (Lorimer et al., 2007b; Keane et al., 2012; Thornton et al., 2013b; Petroff et al., 2015b; Champion et al., 2015a; Spitler et al., 2014a). This is in part because of their unknown flux distribution and location within the radio telescope beam, as well as the low number of observed events. It is further exacerbated by the different specifications of the surveys that find them, whose disparate search algorithms, fluence completenesses, and sensitivity can affect their detection rate. Extrapolating to other frequencies is also difficult since spectral indices and the extent of scattering are still unknown.

[1] http://www.caastro.org/news/2014-utmost

Thornton et al. (2013b) searched about 25% of the High Time Resolution Universe (HTRU) survey data and found four FRBs. They estimated an all-sky daily rate of $1.0^{+0.6}_{-0.5} \times 10^4$ above $\sim$3 Jy ms from 23 days of data and using a 0.55 deg^2 beam. The rate based on HTRU has since come down ($6^{+4}_{-3} \times 10^3$ sky^{-1} day^{-1}) with the discovery of five more FRBs in three times as much data (Champion et al., 2015a). Keane & Petroff (2015) also found a rate that was lower than the initial estimate, calculating $\sim$2500 sky^{-1} day^{-1} after accounting for completeness factors like fluence sensitivity. Though the error bars are still significant, there is some convergence on the rate, and it now seems likely that there are thousands of such events each day at 1.4 GHz.

Event rate estimates at 1.4 GHz are converging, but strong rate constraints have not yet been made in other bands. The non-detection by UTMOST (an upgrade to the Molonglo Observatory Synthesis Telescope) (Caleb et al., 2016b) placed a 2σ upper limit on the number of bright events (10^3 events per sky per day above 11 Jy ms) after searching 467 hours at a fraction of its eventual sensitivity. FRB 110523 remains the only published event not found around 1.4 GHz. It was found near 800 MHz, where scattering or the intrinsic spectral index might have rendered this lower-frequency FRB unobservable. Kulkarni et al. (2015) argued that the steep blue spectrum seen in FRB 121102 (Spitler et al., 2014a) was indicative of free-free absorption, the optical depth of which scales as $\lambda^{2.1}$ and would make metre-wave bursts difficult to see. A greater concern comes from scattering. Sources broadened by scattering to $\sim$10 ms at 1.4 GHz would be $\sim$100 ms at 800 MHz, and a couple of seconds at 400 MHz, due to the λ^4 scaling of the scattering width.

Some surveys that could have great impact on FRB science are threatened by strong scattering. ALERT hopes to localize dozens of bursts with LOFAR after finding them with the large field-of-view (FoV) APERTIF (van Leeuwen, 2014; Verheijen et al., 2008), UTMOST will have $\sim$8 deg^2 of sky coverage 24/7 at 843 MHz (Caleb et al., 2016b),

and HIRAX[2], Tianlai[3] and CHIME (400-800 MHz) could see 10^{2-4} per year, with the ability to write full polarization information (Bandura, 2014). However, their success depends on whether or not the rate of detectable FRBs is comparable to that at higher frequencies.

3.3.1 Implications for the flux distribution

FRB 110523 was found by searching data from the Green Bank Hydrogen Intensity Mapping (GBTIM hereon) survey (Chang et al., 2010; Masui et al., 2015b; Switzer et al., 2013). These data were taken with 1.024 ms cadence between 700-900 MHz using the GBT linearly-polarized prime-focus 800 MHz receiver, along with the GBT Ultimate Pulsar Processing Instrument (GUPPI) digital back-end. An effective DM range of 20-2000 $\mathrm{pc\,cm^{-3}}$ was then searched for FRBs. At each DM, the data were convolved with all possible lengths of top-hat windows up to 100 ms to search for peaks. The peaks were then compared to the root mean square (RMS) of the convolved time-stream, the ratio of which is what we will refer to as signal-to-noise ratio (SNR). The survey duration was 660 hours.

In order to test the observed FRB flux distribution, $N(S)$, we can apply a standard $\log(N)$-$\log(S)$ test. We will consider only power-law distributions of form $N(>S) \propto S^{-\alpha}$. In a Euclidean Universe a population of sources that are uniformly distributed in space should have $N(>S) \propto S^{-3/2}$. This makes intuitive sense, since number counts ought to increase like the cube of distance, while the flux falls off as inverse squared distance. In Sect. 3.5 we apply this test rigorously at 1.4 GHz and discuss the subtleties involved in such a statistic.

With no FRBs found between the search algorithm's detection threshold, 8σ, and 32σ, where FRB 110523 was found, we can test if this has any implications for the true flux distribution. The question we are trying to answer is "Having seen a single event,

[2]http://www.acru.ukzn.ac.za/∼hirax/
[3]http://tianlai.bao.ac.cn/

what is the probability that it has SNR greater than s for a given value of α?". This is given by the ratio of integrals,

$$\beta \equiv \frac{\int_{s_{\max}}^{s_\infty} N(s)ds}{\int_{s_{\min}}^{\infty} N(s)ds}, \tag{3.2}$$

which reduces to $\beta = \left(\frac{s_{\max}}{s_{\min}}\right)^{-\alpha}$ for $\alpha \neq 0$ and integrands of the form $N(s) \propto s^{-\alpha-1}$. This statistic is equivalent to the $V/V_{\max}$ test that has been used to probe the underlying spatial distribution of quasars (Schmidt, 1968a) as well as gamma-ray bursts (Ogasaka et al., 1991). Calculating β as a function of α shows that steep distributions with $\alpha > 2.2$ are ruled out with 95% confidence by this single detection alone.

This is mathematically equivalent to the single-burst solution to a more general approach similar to the biased coin-flip scenario outlined by Connor et al. (2016c). If $M_{\rm high}$ FRBs are observed above a threshold SNR of $s_{\rm thresh}$, with $M_{\rm tot}$ above $s_{\min}$, and p is the relative probability of detecting an FRB in the high-SNR region, then

$$P(M_{\rm high}|\, M_{\rm tot}, p) = \binom{M_{\rm tot}}{M_{\rm high}} p^{M_{\rm high}}(1-p)^{M_{\rm tot}-M_{\rm high}}, \tag{3.3}$$

where p is just $\beta(\alpha)$. Clearly this reduces to the previous result in the case where $M_{\rm high} = M_{\rm tot} = 1$.

3.3.2 How to discuss event rate

The simplest constraints on event rate one can make will be an expected event rate for a future survey with identical parameters. Transferring that rate to another survey or onto the sky requires care, and in both cases uncertainties are introduced that are hard to quantify. For this reason we start by calculating a rate for GBTIM in Sect. 3.3.3, which predicts how many FRBs are expected if an identical survey were to take place again. After that we discuss the implications for other comparable surveys, which should be fairly

robust against things like burst-width sensitivity and the choice of fluence thresholds. In Sect. 3.3.5 we provide an all-sky rate, with several caveats, and discuss the meaning of such a value.

3.3.3 Burst rate

The rate of FRBs implied by 110523 will be independent of its observed brightness. The relevant quantity is the survey sensitivity, so $s_{\min}$ is the only flux scale that should show up in our rate estimate. For a true rate μ_0 above $s_{\min}$, we would expect the number of bursts, M, in a given survey above some SNR, s, to be

$$M_s = \mu_0 \, \Omega \, T_{\rm int} \frac{N(>s)}{N(>s_{\min})}, \tag{3.4}$$

where Ω is the telescope's FoV and $T_{\rm int}$ is the time on sky. We use the rate above some SNR so that we can easily scale it to a rate prediction for a different survey without making any implicit assumption about the distribution of FRBs in flux, fluence, or duration. Similar to Eq. (3.2), this becomes

$$M_s = \mu_0 \, \Omega \, T_{\rm int} \frac{s^{-\alpha}}{s_{\min}^{-\alpha}} \quad \text{for } \alpha > 0. \tag{3.5}$$

However, since we will not try to estimate an all-sky daily rate until Sect. 3.3.5, for now we will take $T_{\rm int}$ and Ω to be in units of the GBTIM on-sky time and beam-size. Therefore M_s should be thought of as the number of FRBs one would expect if the GBTIM were repeated.

Frequentist rate limits

If we regard the sky rate μ_0 as fixed, we can immediately write down the probability of observing $M_{\rm tot}$ FRBs above a SNR of s. It is simply given by the Poissonian distribution

$$P(M_{\rm tot}|\mu_0) = \frac{M_{s_{\rm min}}^{M_{\rm tot}} {\rm e}^{-M_{s_{\rm min}}}}{M_{\rm tot}!}, \tag{3.6}$$

where $M_{s_{\rm min}}$ is given by Eq. (3.5) for $s = s_{\rm min}$. Now we can ask which values of M_s make the observed value of $M_{\rm tot} = 1$ unlikely. Choosing a threshold value of 5%, we can—in this sense—rule out expected event counts $M_{s_{\rm min}}$ outside of the range from 0.05-4.50 events per GBTIM-like survey, with a maximum likelihood value at 1.

Bayesian rate limits

From a Bayesian viewpoint, we want to look at the posterior for the expected number of detections, $M_{s_{\rm min}}$ rather than the likelihood. For simplicity we choose a flat prior on $M_{s_{\rm min}}$, which means that the posterior is again

$$\mathcal{P}(M_{s_{\rm min}}|M_{\rm tot}) = \frac{M_{s_{\rm min}}^{M_{\rm tot}} {\rm e}^{-M_{s_{\rm min}}}}{M_{\rm tot}!}. \tag{3.7}$$

Note that, although the posterior has the same functional form as the likelihood, it is to be read as a density in $M_{s_{\rm min}}$ rather than a probability for $M_{\rm tot}$. Now we can calculate another 95% confidence interval, defined as the smallest interval I with the property $\int_I {\rm d}\mu_0\, \mathcal{P}(\mu_0|M_{\rm tot}) = 0.95$. We find for this 95% confidence interval $I = [0.24,\, 5.57]$ events for a GBTIM-like survey. From hereon we will quote the rate error bars based on the posterior. The posterior for μ_0, which is the same as Eq. (3.7) multiplied by $\Omega\, T_{\rm int}$, is shown in Fig. 3.3.

3.3.4 Implications for other surveys

Though only one event was observed in the 660 hours of archival data, the fact that any burst was detectable in this band is significant. Some of the most important upcoming surveys for FRB science will observe below 1.4 GHz. UTMOST (Caleb et al., 2016b) will be on the sky 24/7 with an $\sim$8 deg^2 FoV and 18,000 m^2 of collecting area, observing at 843

MHz. ALERT hopes to localize dozens of FRBs by first detecting them with the large-FoV APERTIF (van Leeuwen, 2014; Verheijen et al., 2008) and then following up with roughly arcsecond resolution when they arrive several minutes later at LOFAR. Another survey for which FRB 110523's discovery is relevant is CHIME, observing at 400-800 MHz. If the event rate in this band is comparable to the one at higher frequencies, then its large FoV and uninterrupted observing will make it by far the fastest FRB survey.

Since the rate of detection depends on an interplay of the underlying FRB flux and scattering distributions with a survey's thermal sensitivity, fluence completeness, and observing frequencies, the comparison of two surveys with similar specifications is by far the safest bet. CHIME has ∼8,000 m^2 of collecting area compared to GBT's ∼7,850 m^2 and has 100 MHz of overlap with GBTIM. UTMOST will observe within the GBTIM band with similar sensitivity per steradian. Though others (Burke-Spolaor & Bannister, 2014a) have provided models for calculating inter-survey sensitivity based on sky pointing and temporal broadening, we compare only similar telescopes and adopt the simplest possible comparison based on known features of each instrument. Given how little is known about scattering properties and spectral indices, we provide only a skeleton model below; a more detailed calculation is beyond the scope of this paper.

A survey, Σ, that is similar to the GBTIM experiment will see N_Σ events per day based on the one detected burst in ∼27.5 days at GBT. This is given by

$$N_\Sigma = \frac{1}{27.5}\left(\frac{G_\Sigma}{G_{\rm GBT}}\frac{\langle T^{\rm sys}_{\rm GBT}\rangle}{\langle T^{\rm sys}_{\Sigma}\rangle}\sqrt{\frac{B_\Sigma}{B_{\rm GBT}}}\right)^{\alpha}\left(\frac{\Omega_\Sigma}{\Omega_{\rm GBT}}\right)\ {\rm day}^{-1} \tag{3.8}$$

where B gives the survey's bandwidth, G is the gain, and $\langle T^{\rm sys}\rangle$ gives the pointing-averaged system temperature. For GBT we take the effective solid angle based on the full-width half max (FWHM) in power, giving $\Omega_{\rm GBT} \sim 0.055$ $\deg^2$. We use 26.5 K for the sky-averaged system temperature, and a gain of 2 K Jy^{-1}.

As discussed above, in assessing the impact FRB 110523's detection on other surveys, we want to avoid venturing into the unknown. For this reason we consider only the 100 MHz of overlap between CHIME and GBTIM, since that region is known to have a non-zero rate of observable FRBs. For things like beam size, we take the maximum possible FoV based on CHIME's optics and let others adjust the effective solid angle accordingly; though the CHIME collaboration may search only a subset of their primary beam in order to optimize other aspects of their FRB survey, we will estimate the rate based on a full beam.

We model CHIME's primary beam at 750 MHz based on Shaw et al. (2015). A simple dipole beam in the aperture plane is propagated onto the sky by treating the reflector along the cylinder (north-south direction) as a mirror, and by solving the Fraunhofer diffraction problem in the east-west direction. As with GBT, we use only the beam within the half-max contour. This gives $\Omega_{\rm CH} \sim 86$ deg^2 in the middle of its band compared to $\Omega_{\rm GBT} \sim 0.055$ deg^2. Though this gives a ratio of ∼1600 between the two telescope's beam sizes, we remind the reader that this is an approximate solid-angle upper-limit for CHIME between 700-800 MHz. We then estimate its aperture efficiency as 50%, compared with 72% at GBT[4], whose feed horn maximally illuminates its dish while minimizing ground spill, something that is difficult with CHIME's dipole antennas. This makes $G_{\rm CH} = 1.38$ K Jy^{-1}. Finally, keeping with 26.5 K for GBT's system temperature as before and using CHIME's design system temperature of 50K (Bandura, 2014), we can write the maximum-likelihood value for the CHIME rate as

$$N_{\rm CH} \approx 7.5 \left(\frac{50\,{\rm K}}{T^{\rm sys}}\right)^{1.5} {\rm day}^{-1} \tag{3.9}$$

assuming a Euclidean distribution. This means with a 50 K system temperature, CHIME could see between 2-40 (95%) bursts per day if it searches its whole FoV, based on the known non-zero rate above 700 MHz. With a more conservative sky-averaged system

[4]https://science.nrao.edu/facilities/gbt/proposing/GBTpg.pdf

temperature $T^{\rm sys} = 100$ K, CHIME might expect between one every couple of hours and one every two days.

Caleb et al. (2016b) estimate the daily rate of UTMOST in a similar way, directly comparing their sensitivity with that of Parkes at 1.4 GHz. They estimate that they will see a burst once every several days. However, with our constraints on the rate between 700-900 MHz, we can recompute UTMOST's detection rate based on the same band, once it reaches final sensitivity. We use $G = 3.6$ K Jy^{-1}, $T^{\rm sys} = 70$ K, $B = 31.25$ MHz, and a factor of $1/\sqrt{2}$ for its single polarization, based on Caleb et al. (2016b). This gives $4.2^{+19.6}_{-3.2} \times 10^{-1}$ day^{-1}, or between a couple per day and one every couple of weeks. This is consistent with Caleb et al. (2016b).

Finally, we estimate rates for three smaller telescopes related to CHIME. We use $\alpha = 3/2$ and only the 100 MHz of overlap bandwidth with GBTIM, as before. CHIME's Pathfinder, which is made of two 20×37 metre cylinders, has been commissioned over the last two years and now has a working beamforming back-end. If the single formed beam were on sky searching for FRBs at all times, one might expect to detect $0.4 - 9$ per year, taking its beam to be $\Omega_{\rm PF} = 0.62\,{\rm deg}^2$ and $G_{\rm PF} = 0.26$ K Jy^{-1}. The 26 m John A. Galt Telescope, just ∼150 m from the CHIME Pathfinder at the Dominion Radio Astrophysical Observatory (DRAO), could detect $0.1 - 3$ each year, with $\Omega_{26} = 0.78\,{\rm deg}^2$ and $G_{26} = 0.09$ K Jy^{-1}. Another telescope to which a simple FRB back-end could be attached is the 46 m Algonquin Radio Observatory (ARO). This might yield $0.2 - 4.5$ per year, using $\Omega_{\rm ARO} = 0.25\,{\rm deg}^2$ and $G_{\rm ARO} = 0.29$ K Jy^{-1}. Though none of these telescopes makes for a very fast survey, the cost of searching is quite small, and a coincident detection between DRAO and ARO could provide a sub-arcsecond localization.

3.3.5 All-sky daily rate

The standard method for estimating an all-sky rate given a set of observations is to first calculate the rate, μ_0, for that survey — usually the observed number of FRBs divided

by the beam size and the time on sky — and then to scale that based on the survey's sensitivity threshold and a flux distribution index, α. This threshold has typically been in fluence, a physically motivated quantity for FRBs, and is given by

$$H_{\rm min} = \frac{s_{\rm min} \left\langle T^{\rm sys} \right\rangle \tau}{G\sqrt{m\tau B}}, \tag{3.10}$$

where $\langle T^{\rm sys} \rangle$ is the pointing-averaged system temperature, as before, $s_{\rm min}$ is the SNR threshold used in the search algorithm, G is the gain at beam centre, B is the bandwidth, m gives the number of polarizations, and τ is some timescale. If one then wants to quote the rate above, say, 3 Jy ms, then the rate becomes $\mu \times \left(\frac{H_{\rm min}}{3\,{\rm Jy\,ms}}\right)^{\alpha}$.

One problem with this method is that it is not entirely obvious how to choose τ, and several groups have approached it differently. Keane & Petroff (2015) discuss some of these effects and decided to use the value at which their survey becomes fluence complete, 2 Jy ms, based on the maximum width to which they are sensitive. Rane et al. (2016) use sampling time, which is the minimum possible effective burst width. This will maximise the reported search sensitivity because it uses the lowest possible fluence limit, and therefore generically lowers the final rate estimate after scaling to a common fluence. A more exact approach is to quote the rate above some fluence curve $H \propto \sqrt{\tau}$ between $\tau_{\rm min}$ and $\tau_{\rm max}$ corresponding to the actual SNR threshold if white noise is assumed. This is similar to what Champion et al. (2015a) do, who quote their rate above a fluence range.

Since the primary goal of this paper is to compare between surveys, we do not attempt to derive a strict fluence threshold for GBTIM and to scale our all-sky rate based on it. Until the fluence and width distributions for FRBs are known along with a search algorithm's width response, the all-sky rate quoted for some incomplete region of fluence space is not overly useful. Instead, we calculate the rate above our true threshold, which is $s_{\rm min} = 8$ for DMs between 20-2000 pc cm^{-3} and widths between one and two hundred milliseconds. A useful estimate of the rate is given by the maximum of Eq. (3.7),

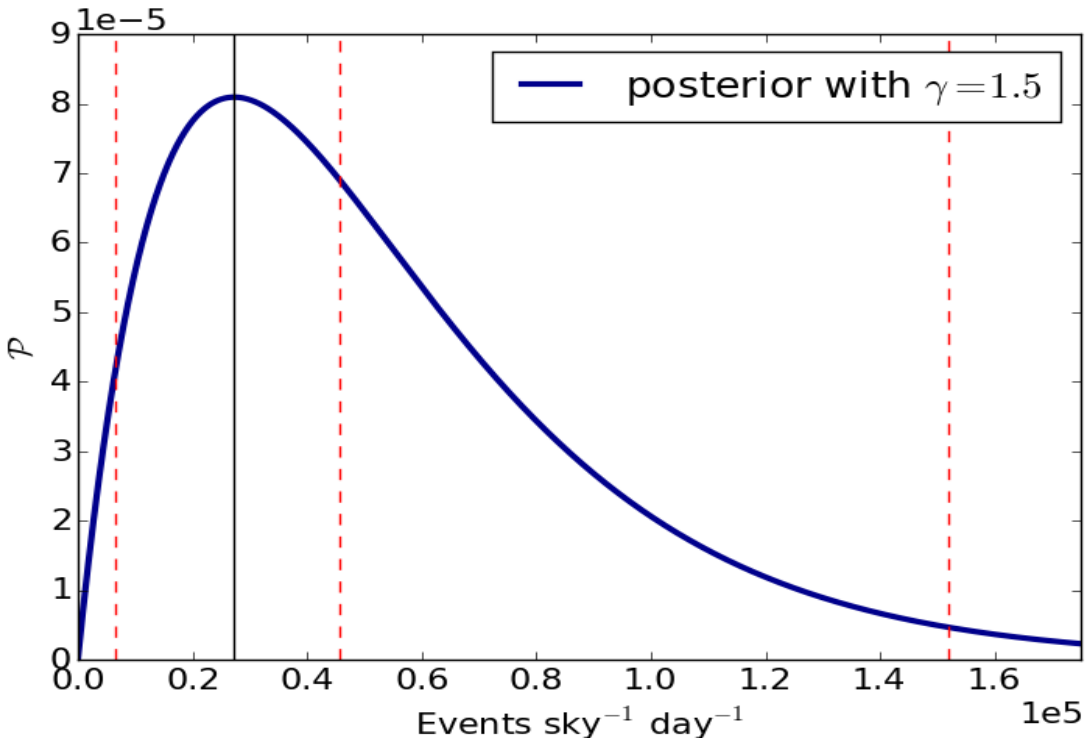

Figure 3.3: Posterior distribution for the all-sky daily rate based on seeing one burst in 27.5 days of data with a 0.055 deg^2 beam. This posterior is meant to be interpreted as the number of FRBs one would see if GBTIM-like surveys were able to observe the whole sky for a day, i.e. we have not scaled the rate based on fluence sensitivity for reasons described in Sect. 3.3.5. The maximum a posteriori value is denoted by the black vertical line, which is at $\sim 2.7 \times 10^4$ sky^{-1} day^{-1}. The two outside blue lines enclose 95% of the curve and the middle blue line denotes the median.

$\mu_0 = \frac{1}{\Omega T_{\rm int}} \left(\frac{s}{s_{\rm min}}\right)^{\alpha}$, for $s = s_{\rm min}$. The all-sky rate for GBTIM above 8σ is then $2.7^{+12.4}_{-2.1} \times 10^4$ sky^{-1} day^{-1}, between 700-900 MHz. We plot the corresponding posterior in Fig. 3.3.

Though this value seems high, GBTIM is a sensitive survey, with $F_{\rm min} = 97$ mJy for a 3 ms pulse. Without making any concrete statements about our sensitivity in fluence space, we can get an idea of how this rate compares to the estimates from other surveys based only on thermal sensitivity. We can use the rate inferred from the 9 HTRU FRBs as a baseline (Champion et al., 2015a). If we assume the width completeness of various surveys is roughly similar, we can tether our rate to the HTRU one, and calculate a

sensitivity ratio, r_s. Comparing Parkes and GBT, this will be

$$r_s = \frac{\langle T_{\rm H}^{\rm sys} \rangle}{\langle T_{\rm GBT}^{\rm sys} \rangle} \frac{G_{\rm GBT}}{G_{\rm H}} \sqrt{\frac{B_{\rm GBT}}{B_{\rm H}}} \frac{s_{\rm min}^{\rm H}}{s_{\rm min}^{\rm GBT}}. \tag{3.11}$$

Using $s_{\rm min}^{\rm H} = 10$, an average on-axis gain of $G_{\rm H} = 0.64\,{\rm K\,Jy^{-1}}$, $B_{\rm H} = 340\,{\rm MHz}$, and a 23 K system temperature (Keith et al., 2010a), we find $r = 2.60$. Our rate can then by multiplied by $r^{-\alpha}$, which gives $6.4^{+29.5}_{-5.0} \times 10^3\,{\rm sky^{-1}\,day^{-1}}$, assuming a Euclidean distribution.

This is an extrapolation of our rate estimate at 700-900 MHz to 1.4 GHz. It corresponds to the number of FRBs that HTRU should be detecting if the intrinsic rates of FRBs in the two frequency bands were the same. This extrapolated rate is indeed consistent with the rate observed by HTRU, which shows that the rate of FRBs detectable at low frequencies is not significantly lower than at 1.4 GHz, which was not previously obvious due to the threat of scattering and steep blue power-laws (Kulkarni et al., 2015). This result makes the aforementioned upcoming low-frequency surveys especially promising for FRB science.

This is also consistent with the non-detection upper-limit set by Caleb et al. (2016b), who found the rate to be below $10^3\,{\rm sky^{-1}\,day^{-1}}$ for one-millisecond 11 Jy bursts at the 2σ level. This was based on two surveys, one with 467 hours on sky, and another with 225 hours on sky at roughly twice the sensitivity. Comparing their time-weighted thermal sensitivity with GBTIM, we get $r_s \approx 10^2$, making our 95% upper-limit a few hundred per sky per day.

3.4 Latitudinal dependence

There is now evidence that the FRB rate is nonuniform on the sky, with fewer detectable events at low Galactic latitudes (Burke & Graham-Smith, 2014). However the statistical significance of this finding may be overestimated. Petroff et al. (2014) compute

the probability of the disparity between the number of bursts seen in the high- and intermediate-latitude ($|b| < 15°$) components of the High Time Resolution Universe survey (HTRU). They calculate the probability of seeing $N = 0$ in the intermediate latitude survey and $M = 4$ in the high-latitude, despite having searched 88% more data in the former, and they rule out the uniform sky hypothesis with 99.5% certainty. We would point out that in general $P(N|M)$ describes a very specific outcome, and it would be more appropriate to include all outcomes equally or more unlikely. That number might also be multiplied by two, since if the survey found four intermediate-latitude FRBs and zero high-lat ones, we would ask the same question.

But a simpler approach to this problem would be analogous to a series of coin flips. If a coin were flipped four times, the probability of seeing all heads is 1/16, or 6.25%. This is a factor of six higher than the analogous analysis of Petroff et al. (2014). We can test the null hypothesis that the coin is fair, and using the binomial statistic would conclude that the outcome is consistent with a fair coin at 95% confidence, differing from the conclusion of Petroff et al. (2014). In the FRB case the Universe is flipping a coin each time a new burst appears, with some bias factor due to things like different integration times. HTRU has since reported five more bursts in the high Galactic region, but using a dataset that spent ∼2.5 times more time at high latitudes. Below we try and quantify the likelihood of this.

If one wants to compare two statistical hypotheses, then the claims of each should be treated as true and their likelihood discrepancy should be computed. In the case of testing the abundance of FRBs at high latitudes, the sky should be partitioned into high and low regions a priori (e.g., the predefined high-latitude HTRU and its complement). The rate in both regions is then taken to be the same, and the likelihood of a given spatial distribution of observed sources can be calculated. This situation is naturally described by a biased binomial distribution with a fixed number of events. Suppose a total of K FRBs are observed in a given survey. We can ask the question, what is the probability

of seeing M events in the high region and $(K - M)$ events in the lower region? This probability can be calculated as

$$P(M|\, K, p) = \binom{K}{M} p^M (1-p)^{K-M}, \tag{3.12}$$

where p is the probability that an event happens to show up in the high region. In a survey where more time is spent on one part of the sky than the other, $p = \alpha/(\alpha + 1)$, where α is the ratio of time spent in the high-latitude region vs. the intermediate region. In the case of the HTRU survey, $K = 9$ and since none were found in the low-latitude region, $M = 9$. Roughly 2500 hours were spent searching the upper region and ∼1000 hours were spent at $|b| < 15°$, giving $\alpha = 2.5$. Using Equation 3.12, this outcome is only ∼5% unlikely.

The problem is given a quasi-Bayesian treatment by Petroff et al. (2014), which gives the following.

$$P(N|\, M) = \alpha^N (1+\alpha)^{-(1+M+N)} \frac{(M+N)!}{M!N!} \tag{3.13}$$

This gives a probability of ∼3.5%, using all nine FRBs. This method is Bayesian in the sense that they marginalize over the unknown rate and calculate a likelihood, but they then calculate a confidence and do not look at a posterior.

The most obvious difference between the approach we have offered (biased coin-flip) and the quasi-Bayesian method is that we take $M + N$ to be fixed. It follows to ask whether or not we *should* regard the total number of FRBs as "given"? We believe the answer is yes, since this is one of the few quantities that we have actually measured, along with M and N. What we are really trying to infer is how much larger $\mu_{\rm high}$ is than $\mu_{\rm low}$, so these rates should not be marginalized over.

To consider only the likelihood can give misleading results. For example, as more and more FRBs are detected, the likelihood of the particular observed values for N and

M will become smaller and smaller, due to the sheer number of possible tuples (N, M). To decide whether or not there is evidence for FRBs to occur with a higher probability at high latitudes, we can instead use the formalism of Bayesian model selection. This formalism does not aim to rule out a particular model, it only compares the validity of two models. For this, we formulate two specific models, Model 1 in which we assume that $p_1 = \alpha/(1+\alpha)$ as above (i.e. uniform rate across the sky), and Model 2 in which we regard p as a free parameter, equipped with a flat prior between 0 and 1. The model selection will then be based on the comparison of the posterior probabilities for the two models,

$$\frac{P(\text{Model 1}|M,K)}{P(\text{Model 2}|M,K)} = \frac{P(M|\text{Model 1},K)}{P(M|\text{Model 2},K)}, \tag{3.14}$$

where we have assumed equal prior weights for the two models. Using the binomial likelihood, Eq. (3.12), and marginalizing over the unknown probability p in the case of Model 2, this ratio is easily calculated to be

$$\frac{P(M|\text{Model 1},K)}{P(M|\text{Model 2},K)} = (K+1)\binom{K}{M} p_1^M \ (1-p_1)^{K-M}\,. \tag{3.15}$$

For the observations discussed above with $M = K = 9$ and $\alpha = 2.5$, we find a ratio of 0.48, so there is no strong preference for either of the two models.

3.5 Is the distribution Euclidean?

An observable distinction between cosmological models and more local models for the FRB population is given by the distribution of flux densities. This is independent of the pulse dispersion. The simplest model is one in which FRBs are uniformly distributed and their location does not influence any of their observable properties other than that farther bursts appear dimmer. In Euclidean space this leads to an unambiguous prediction for

their flux densities, namely

$$\mathrm{d}N \propto S^{-(\alpha+1)}\,\mathrm{d}S \tag{3.16}$$

with $\alpha = 3/2$, where S is the flux density and $\mathrm{d}N$ is the number of FRBs with a flux density in an infinitesimal interval $\mathrm{d}S$. This relation holds independently from their intrinsic luminosity distribution and does not require them to be standard candles. Deviations from an index 3/2 are for example expected if the number density of FRBs is not constant and/or if their distances are large enough that deviations from Euclidean geometry become important. If FRBs are extragalactic, but local, then the default expectation should be $\alpha = 3/2$. It is worth noting that a constant-density Euclidean distribution is the only model that leads to a clear prediction for the observed flux densities. If FRBs are at large enough distances that the expansion history of the Universe is important, then the population of FRBs can be expected to also have undergone some evolution, thus introducing functional degrees of freedom that are at present completely unconstrained. An additional effect that can in principle influence the measured distribution of flux densities is dispersion smearing, i.e., the dispersion of the pulses' arrival times within a frequency bin of a survey, resulting in a reduction of the signal-to-noise ratio for very high dispersion measures. If dispersion measures were correlated with distance, this could potentially lead to a systematic flattening of the distribution, but will not affect its shape if the dispersion measure and distance of an FRB are uncorrelated.

In this section we investigate whether the constant-density Euclidean model is consistent with current observations. We do this by studying the one-parametric class of models in which α is a free parameter and which includes the constant-density Euclidean model as a special case. Deriving the observational constraints on the parameter α has the potential of showing that $\alpha = 3/2$ is disfavoured by the data without the need to make any more complicated model assumptions. We derive constraints from a combination of source counts of different surveys and the observed V/V_{max}-values (Schmidt, 1968b).

In the simple constant-density Euclidean model, the power-law behaviour of Eq. (3.16) is not only valid for the flux densities, but also for any other observable that depends linearly on flux density. One example would be the fluence

$$\begin{aligned} F &= \int \mathrm{d}t\, S(t) \\ &= S\,\tau, \end{aligned} \tag{3.17}$$

where τ is the duration of a burst and S is the average flux density within the interval of length τ. Another example is the observed signal-to-noise ratio, which depends on the flux density of the burst, its duration, and of course on properties of the telescope and the survey. In many cases it can be approximated as

$$s \approx K\, S\, \tau^{1/2}, \tag{3.18}$$

where we include all instrumental properties in the constant K (e.g., Caleb et al., 2016a). The detection of an FRB is always subject to a sensitivity cutoff in signal-to-noise, and not in flux density or fluence. This makes the statistics of flux density and fluence more complicated than the statistics of the signal-to-noise ratio s and we choose to cast all equations in terms of s. Note that, as is common in the field, we use the term signal-to-noise ratio to mean the amplitude of the FRB signal plus noise, divided by the standard deviation of the noise, which can be approximately determined empirically for each search window length τ.

We derive the necessary statistical methodology in the following section, discuss the data that we use and show our results in Sect. 3.5.2.

3.5.1 Methodology

Likelihood for the observed signal-to-noise ratios

Clearly some information on the parameter α is contained in the distribution of observed signal-to-noise ratios. If we assume a value for α and suppose that a survey with a given signal-to-noise threshold $s_{\min}$ detects an FRB, then the likelihood for its signal-to-noise ratio to be s is, according to Eq. (3.16),

$$\mathcal{P}(s|s_{\min},\alpha) = \begin{cases} \frac{\alpha}{s_{\min}} \left(\frac{s}{s_{\min}}\right)^{-(\alpha+1)} & \text{if } s \geq s_{\min} \\ 0 & \text{else} \end{cases} . \tag{3.19}$$

If the survey detects n independent FRBs then the joint likelihood for their signal-to-noise ratios is simply the product of the individual ones.

For N different surveys, each detecting $n_1, \ldots, n_N$ FRBs, the situation is the same, except that we have to take into account that each survey has a different detection threshold $s_{\min}$. If we denote the observed signal-to-noise value of the i-th FRB in the I-th survey as $s_{I,i}$, the $(n_1 + \cdots + n_N)$-dimensional vector of all these observed values as $\vec{s}$, the N-dimensional vector of all threshold signal-to-noise values as $\vec{s}_{\min}$, and the N-dimensional vector of the numbers of detections in each survey as $\vec{n}$, the complete likelihood becomes

$$\mathcal{P}(\vec{s}|\vec{n},\vec{s}_{\min},\alpha) = \prod_{I=1}^{N} \prod_{i=1}^{n_I} \mathcal{P}(s_{I,i}|s_{\min,I},\alpha). \tag{3.20}$$

This is easily calculated and we will do so in Sect. 3.5.2. In the following we will refrain from mentioning $\vec{s}_{\min}$ explicitly in the notation of probabilities and imply that all survey properties are always fixed.

Note that the combination $(s/s_{\min})^{-\alpha}$ for $\alpha = 3/2$ corresponds to the ratio of the volume interior to the FRB and the volume in which this particular FRB could have been detected by the survey, $V/V_{\max}$, for a constant source density in three-dimensional Euclidean space. The likelihood we are using here to constrain α is thus closely related

to the $V/V_{\max}$-test used in many contexts to check for deviations from a constant density for a source population (e.g., Schmidt, 1968b).

Likelihood for the number of observed FRBs

In addition to the information contained in the signal-to-noise ratios of the observed bursts, some information is also contained in the numbers of bursts detected by different surveys. For any one survey, the number of detected FRBs puts constraints on the rate of FRBs occurring above the detection threshold of that survey. This rate can be rescaled to a different survey with a different detection threshold and confronted with the observed number of bursts for that survey. However, the rescaling depends on the parameter α and thus the number of bursts detected by two or more surveys puts constraints on α.

To include these constraints in our analysis we introduce the FRB rate explicitly as an unknown parameter. Since the rate observable by a given survey depends on various properties of the survey, we define the rate r_0 occurring above the detection threshold of a hypothetical survey described by a system temperature $T_{\mathrm{sys},0} = 1\,\mathrm{K}$, a gain $G_0 = 1\,\mathrm{K\,Jy^{-1}}$, $n_{\mathrm{p},0} = 2$ observed polarizations, a bandwidth $B_0 = 1\,\mathrm{MHz}$, and a signal-to-noise threshold $s_{\min,0} = 1$. As explained by Connor et al. (2016a), the FRB rate above the detection threshold of the I-th survey is then a rescaled version of this rate, namely

$$\begin{aligned} r_I &= r_0 \left(\frac{T_{\mathrm{sys},I}}{T_{\mathrm{sys},0}} \frac{G_0}{G_I} \sqrt{\frac{n_{\mathrm{p},0}\, B_0}{n_{\mathrm{p},I}\, B_I}} \frac{s_{\min,I}}{s_{\min,0}} \right)^{-\alpha} \\ &= r_0 \left(\frac{T_{\mathrm{sys},I}}{G_I} \sqrt{\frac{2\,\mathrm{MHz}}{n_{\mathrm{p},I}\, B_I}}\, s_{\min,I}\,\mathrm{Jy} \right)^{-\alpha} . \end{aligned} \tag{3.21}$$

The expected number of FRBs detected by the I-th survey will then be

$$M_I = r_I\, \Omega_I\, T_I, \tag{3.22}$$

where Ω_I is the angular size of the survey's field of view and T_I is the time spent surveying. The likelihood for the actual number of FRBs observed in this survey is then a Poissonian distribution with this expectation value,

$$P(n_I|r_0,\alpha) = \frac{{M_I}^{n_I}}{n_I!}\,\mathrm{e}^{-M_I}. \tag{3.23}$$

For N surveys the complete likelihood again becomes a product of the likelihoods for the individual surveys,

$$P(\vec{n}|r_0,\alpha) = \prod_{I=1}^{N} P(n_I|r_0,\alpha), \tag{3.24}$$

and can be used to put constraints on the distribution of flux densities via the parameter α, as well as on the overall rate of FRBs, here parameterized as the rate above the detection threshold of our hypothetical survey, r_0.

Posterior

To get the complete set of constraints on the distribution of flux densities, both from the observed signal-to-noise ratios and from the detection numbers of different surveys, we combine the results of Sects. 3.5.1 and 3.5.1. We write the joint likelihood for the number of observed FRBs and their signal-to-noise ratios as

$$\begin{aligned}\mathcal{P}(\vec{s},\vec{n}|r_0,\alpha) &= \mathcal{P}(\vec{s}|\vec{n},r_0,\alpha)\,P(\vec{n}|r_0,\alpha)\\ &= \mathcal{P}(\vec{s}|\vec{n},\alpha)\,P(\vec{n}|r_0,\alpha).\end{aligned} \tag{3.25}$$

If we assume flat priors for r_0 and for $\alpha > 0$, this likelihood is proportional to the joint posterior for the parameter α and the rate r_0.

The likelihood for observed fluxes within a survey obviously only gives us constraints if the survey has in fact detected at least one FRB. Note, however, that we can in principle

include surveys without FRB detection by setting

$$\mathcal{P}(\vec{s}|n = 0, s_{\min}, \alpha) = 1 \tag{3.26}$$

and thus still use them to constrain the parameter α via their implications on the FRB rate above their detection thresholds. Similarly, the numbers of FRBs detected by different surveys only have implications for the parameter α if we assume that the surveys observe the same source population, described by the same rate r_0. This assumption will in general be violated if different surveys have different frequency coverage or different observational strategies. Specifically, the observations of a deep and narrow survey will in general not be described by the same statistics as those of a shallow and wide survey, as explained by Connor et al. (2016b). Care is thus warranted when comparing detection numbers of qualitatively different surveys. Such an attempt will require more parameters or simply setting

$$P(n|r_0, \alpha) = 1 \tag{3.27}$$

for all surveys that are not expected to be described by r_0.

3.5.2 Data and results

We make use of 15 observed FRBs from seven surveys. For definiteness, we list all values used in our calculation in Tables 3.1 and 3.2. For the likelihood of the numbers of detected FRBs, we only make use of two dedicated pulsar surveys with well-defined characteristics, namely the High Time Resolution Universe Pulsar Survey (HTRU; Keith et al. 2010b) at the Parkes telescope and the Pulsar ALFA survey (PALFA; Cordes et al. 2006) at the Arecibo Observatory. We choose these two surveys because for most other discovered FRBs it is hard to estimate the surveying period T that has been searched for FRBs, especially in the case of non-detections. The survey of Masui et al. (2015a) is similarly well-defined, but sensitive to different frequencies. We assume our parameter

r_0 to describe the rate at frequencies around 1.4 GHz and do not want to make any assumption about the relation between this rate and the rate at 800 MHz, which is the central frequency of Masui et al. (2015a).

Even for HTRU and PALFA, the parameters needed in Eq. (3.21) are defined somewhat ambiguously. To avoid building complicated models of the telescopes and surveys, we generally opt for simple choices that can be made consistently for both surveys. Specifically, this means that we do not include any estimate of the sky temperature due to the Milky Way in the values we assume for the system temperature T_{sys}. For the gain G we use the arithmetic mean of the gains corresponding to the beam centres of the multi-beam receivers. The bandwidth B does not include frequencies deemed unusable by the surveying team and the angular size of the field of view Ω is intended to approximate the area within the half-maximum beam power. The resulting numerical values are listed in Table 3.1. Other reasonable choices for these parameters will typically lead to deviations on the order of 10%. Note that the exact definition of each parameter does not impact the results as long as the same definition is used for all surveys that are being compared.

For the constraint on α coming from the likelihood for the observed signal-to-noise ratios, we can use all detected FRBs, as long as there is a well-defined signal-to-noise cutoff s_{min}. Since we are investigating the population of sources, we are not including repeated bursts from the same object (Spitler et al., 2016b). We also exclude the single burst detections by Lorimer et al. (2007a) and Keane et al. (2011), since no definitive value of s_{min} can be determined. We list the values of s and s_{min} that we use in Table 3.2.

After calculating the two-dimensional posterior for α and r_0, we derive the final constraint on α by marginalising over r_0 and vice versa. These posterior distributions are shown in Fig. 3.4.

Figure 3.4 shows a strong correlation between the FRB rate and the slope parameter α. This can be understood in terms of regions of parameter space that are in tension with the data. If the rate of FRBs is high, a shallow flux density distribution will overpredict

Table 3.1: Parameters assumed for the FRB surveys. See Sect. 3.5.1 for the meaning of the symbols.

survey[1]	$s_{\min}$	$T_{\rm sys}$/K	G/(K/Jy)	$n_{\rm p}$	B/MHz	Ω/(deg^2)	T/h	n
HTRU [1]	10	23	0.64	2	340	13×0.043	3650	9
PALFA [2]	7	30	8.5	2	300	7×0.0027	886	1

[1] [1] Champion et al. 2015b; Thornton et al. 2013a; Keith et al. 2010b; [2] Spitler et al. 2014b; Cordes et al. 2006

Table 3.2: Parameters of each individual FRB used in our calculation. The signal-to-noise ratios s are taken from the FRBcat website[1] (Petroff et al., 2016).

name	s	$s_{\min}$	survey[2]
FRB090625	30	10	[1]
FRB110220	49	10	[1]
FRB110626	11	10	[1]
FRB110703	16	10	[1]
FRB120127	11	10	[1]
FRB121002	16	10	[1]
FRB130626	21	10	[1]
FRB130628	29	10	[1]
FRB130729	14	10	[1]
FRB121102	14	7	[2]
FRB010125	17	7	[3]
FRB131104	30	8	[4]
FRB140514	16	10	[5]
FRB150418	39	10	[6]
FRB110523	42	8	[7]

[1] `http://www.astronomy.swin.edu.au/pulsar/frbcat/`

[2] [1] Champion et al. 2015b; Thornton et al. 2013a; Keith et al. 2010b; [2] Spitler et al. 2014b; Scholz et al. 2016b; [3] Burke-Spolaor & Bannister 2014b; [4] Ravi et al. 2015; [5] Petroff et al. 2015a; [6] Keane et al. 2016b; [7] Masui et al. 2015a; Connor et al. 2016a

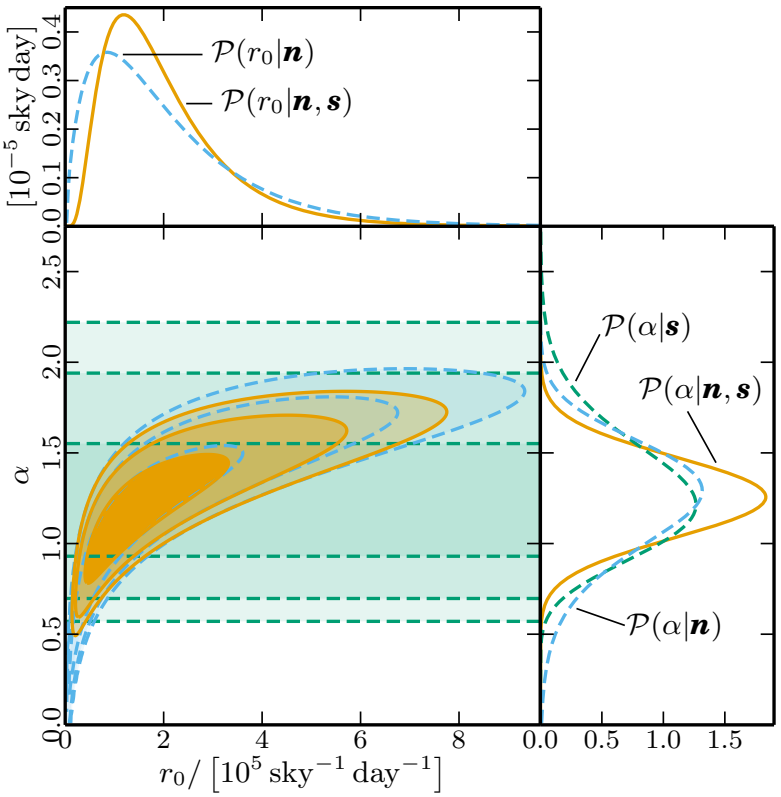

Figure 3.4: Posterior distribution for the parameter α describing the distribution of FRB flux densities and the FRB rate r_0. The bottom left panel shows the two-dimensional posterior for both parameters, the smaller panels show the marginalised posteriors for each parameter individually. We show separate curves and contours for the constraints coming from the signal-to-noise ratios $\mathbf{s}$ (green dashed), from the detection numbers $\mathbf{n}$ (blue dashed), and their combination (orange solid). The contour lines show the 68%, 95%, and 99% confidence regions.

the number of FRBs occurring at high signal-to-noise ratios. If the rate is low, on the other hand, a steep distribution will underpredict the number of FRBs occurring above the detection threshold of current surveys, especially at high signal-to-noise values.

The figure also shows the posterior distributions that are obtained if only the detection numbers or the signal-to-noise ratios are used, instead of their combination. Obviously, the signal-to-noise ratios alone do not constrain the FRB rate at all. Thus, the corresponding contours appear as horizontal lines in the main panel of the figure. And even for the parameter α, the main constraint comes from the comparison of the detection num-

bers for the two surveys HTRU and PALFA. Using the signal-to-noise ratios in addition does, however, add some information, in that it rules out close-to-flat flux distributions and very low rates.

The full posterior for the parameter α still allows a wide range of values. The 95% confidence interval is

$$0.8 \leq \alpha \leq 1.7. \tag{3.28}$$

This is to be contrasted with recent results from the literature. Caleb et al. (2016a), for example, find $\alpha = 0.9 \pm 0.3$ and Li et al. (2016) claim $\alpha = 0.14 \pm 0.20$. We stress that our constraints are model-independent in the sense that we have not assumed any specific relation between flux density, burst duration, and dispersion measure. An important conclusion of our analysis is that the simplest possible model for the distribution of FRBs, constant density in Euclidean space, is consistent with current data. Of course this does not mean that it is proven to be correct, but it does mean that any extension to this model is not data-driven but has to be motivated independently. This finding is consistent with the qualitative conclusions of Katz (2016c) and Katz (2016a).

As a byproduct of our attempt to constrain α, we also obtain constraints on the rate of FRBs at 1.4 GHz. The 95% confidence interval for our parameter r_0 is

$$4.8 \times 10^4\,\mathrm{sky}^{-1}\,\mathrm{day}^{-1} \leq r_0 \leq 5.3 \times 10^5\,\mathrm{sky}^{-1}\,\mathrm{day}^{-1}. \tag{3.29}$$

It may be worth noting that the constraints on the FRB rate tighten up somewhat if the parameter α is fixed. In the constant-density Euclidean model, for example, the 95% confidence limit on the rate is

$$1.6 \times 10^5\,\mathrm{sky}^{-1}\,\mathrm{day}^{-1} \leq r_{0,\alpha=3/2} \leq 5.4 \times 10^5\,\mathrm{sky}^{-1}\,\mathrm{day}^{-1}. \tag{3.30}$$

For any specific survey this rate has to be rescaled according to Eq. (3.21). As an example

we calculate the FRB rate above the detection threshold of the HTRU survey, again for $\alpha = 3/2$,

$$1.9 \times 10^3\,\mathrm{sky}^{-1}\,\mathrm{day}^{-1} \leq r_{\mathrm{HTRU},\alpha=3/2} \leq 6.3 \times 10^3\,\mathrm{sky}^{-1}\,\mathrm{day}^{-1}. \tag{3.31}$$

These are slightly lower values than the range derived by Champion et al. (2015b). We stress again that all rates we calculate are subject to a signal-to-noise cutoff. Converting them to rates above a given fluence is impossible without making further assumptions.

3.6 Conclusions

The search for FRBs with multiple surveys that have disparate sensitivities, frequency coverage, and survey strategy (not to mention non-publication bias), has made dealing with their statistics non-trivial. This is exacerbated by the small number of detected events. In the case of repetition, we remind the reader that several non-cataclysmic models for FRBs are expected to repeat. For supergiant pulses from pulsars, SGR radio flares, or even Galactic flare stars, it is possible that this repetition would be non-stationary and might exhibit strong correlations in time. We have shown that if the repetition had some associated flicker noise and its power spectrum were $1/f^{\gamma}$, then one should expect the repetition rate to be higher immediately after the initial FRB detection. Therefore follow-up observations to archival discoveries that take place years or months after the first event would not provide strong upper limits. This would also mean that if no burst is found in a given beam after some integration time, then it is unlikely that one will occur in the following integration, and therefore a new pointing should be searched. In other words, shallow fast surveys would be favourable.

In Sect. 3.4 we offered a simple way of quantifying the latitudinal dependence of FRBs with a binomial distribution. This is akin to a biased coin flip, in which we ask "what is the probability of M bursts being found in one region and N bursts in its complement, given α times more time was spent in the former". We argue that the jury

is still out on the severity of the latitudinal dependence. With current data the preference for FRBs to be discovered outside of the plane seems consistent with sky-temperature effects and increased scattering, or even pure chance. Whether or not more sophisticated explanations (e.g., Macquart & Johnston 2015) are required remains to be seen. We also provided a Bayesian framework for model comparison, which can be used in the limit where large numbers of FRBs have been detected.

Estimating rates is another statistical challenge. FRB 110523 is the only FRB to be observed below 1.4 GHz. Its detection is encouraging because there are several upcoming surveys below a GHz whose impact on FRB science is hard to overestimate, so long as the transients are detectable at low frequencies. In the next several years CHIME, HIRAX, Tianlai, UTMOST, and ALERT could increase the number of detected FRBs by orders of magnitude, provide polarization information and repetition statistics, and localize them. In Sect. 3.3 we have provided the first detailed bounded constraints on the FRB rate below 1.4 GHz.

We have shown two ways of estimating the rate given the detection of FRB 110523, one based on a frequentist hypothesis test, and the other done in a Bayesian framework. These give the same maximum-likelihood value, but somewhat different 95% confidence intervals. We have then used the GBTIM estimate to forecast rates for CHIME and UTMOST, explicitly only comparing surveys with similar specifications. We find CHIME could detect between 2 and 40 per day, given by $\approx 7.5 \left(\frac{50\,\mathrm{K}}{T^{\mathrm{sys}}}\right)^{1.5}$ day^{-1}, making it the fastest upcoming survey. UTMOST, which observes in a band inside GBTIM's and whose sensitivity per steradian should eventually be comparable, could see between a couple per day and one every two weeks. We also found that CHIME Pathfinder's single formed beam, the nearby 26 m John A. Galt Telescope, and the 46 m ARO might see a couple FRBs each year, providing sub-arcsecond localisation through VLBI.

The difficulties of estimating an all-sky rate above a single fluence value was discussed. We showed how an on-sky rate not attached to a specific survey is not only hard

to predict but also hard to interpret. For that reason we estimated a rate above the true threshold for GBTIM — an SNR of 8 — which gave us $2.7^{+12.4}_{-2.1} \times 10^4\,\mathrm{sky}^{-1}\,\mathrm{day}^{-1}$. The fluences to which GBTIM was sensitive are those above the curve $0.17\sqrt{(\tau/\mathrm{ms})}\,\mathrm{Jy\,ms}$ for pulse widths between 1-100 ms. To test the agreement between this rate and those found by other surveys, we scaled based only on thermal sensitivity. If we extrapolate from this daily rate to a survey with the sensitivity of HTRU, we find $6.4^{+29.5}_{-5.0} \times 10^3\,\mathrm{sky}^{-1}\,\mathrm{day}^{-1}$, which is consistent with (Champion et al., 2015a). We also investigated the flux distribution index, α, at 800 MHz and found that steep distributions with $\alpha > 2.2$ are ruled out. This is consistent with the 1.4 GHz constraints.

3.7 Discussion

Bibliography

Bagchi, M., Nieves, A. C., & McLaughlin, M. 2012, MNRAS, 425, 2501

Bandura, K. e. a. 2014, in Society of Photo-Optical Instrumentation Engineers (SPIE) Conference Series, Vol. 9145, Society of Photo-Optical Instrumentation Engineers (SPIE) Conference Series, 22

Barrau, A., Rovelli, C., & Vidotto, F. 2014, Phys. Rev. D, 90, 127503

Becker, W., Kramer, M., Jessner, A., et al. 2006, ApJ, 645, 1421

Berger, P., Newburgh, L. B., Amiri, M., et al. 2016, ArXiv e-prints, arXiv:1607.01473

Bower, G. C., Deller, A., Demorest, P., et al. 2014, ApJ, 780, L2

Burke, B. F., & Graham-Smith, F. 2014, An Introduction to Radio Astronomy

Burke-Spolaor, S., Bailes, M., Ekers, R., Macquart, J.-P., & Crawford, III, F. 2011, ApJ, 727, 18

Burke-Spolaor, S., & Bannister, K. W. 2014a, ApJ, 792, 19

—. 2014b, ApJ, 792, 19

Caleb, M., Flynn, C., Bailes, M., et al. 2016a, MNRAS, 458, 708

—. 2016b, ArXiv e-prints 1601.02444, arXiv:1601.02444

Champion, D. J., Petroff, E., Kramer, M., et al. 2015a, ArXiv e-prints 1511.07746, arXiv:1511.07746

—. 2015b, ArXiv e-prints, arXiv:1511.07746

—. 2016, MNRAS, arXiv:1511.07746

Chang, T.-C., Pen, U.-L., Bandura, K., & Peterson, J. B. 2010, Nature, 466, 463

Connor, L., Lin, H.-H., Masui, K., et al. 2016a, MNRAS, 460, 1054

Connor, L., Pen, U.-L., & Oppermann, N. 2016b, MNRAS, 458, L89

—. 2016c, MNRAS, arXiv:1601.04051

Connor, L., Sievers, J., & Pen, U.-L. 2016d, MNRAS, 458, L19

Cordes, J. M., Bhat, N. D. R., Hankins, T. H., McLaughlin, M. A., & Kern, J. 2004, ApJ, 612, 375

Cordes, J. M., & Wasserman, I. 2015, ArXiv e-prints 1501.00753, arXiv:1501.00753

—. 2016, MNRAS, 457, 232

Cordes, J. M., Freire, P. C. C., Lorimer, D. R., et al. 2006, ApJ, 637, 446

Danish Khan, M. 2014, ArXiv e-prints, arXiv:1404.5080

Dennett-Thorpe, J., & de Bruyn, A. G. 2002, Nature, 415, 57

Dodin, I. Y., & Fisch, N. J. 2014, ApJ, 794, 98

Drake, S. 1978, Galileo at work : his scientific biography

Falcke, H., & Rezzolla, L. 2014, A&A, 562, A137

Faraday, M., & Martin, T. 1936, Faraday's Diary: Nov. 24, 1855-Mar. 12, 1862, Vol. 7 (G. Bell and sons, ltd.)

Goldreich, P., & Sridhar, S. 2006, ApJ, 640, L159

Hewish, A., Bell, S. J., Pilkington, J. D. H., Scott, P. F., & Collins, R. A. 1968, Nature, 217, 709

Hippke, M., Domainko, W. F., & Learned, J. G. 2015, ArXiv e-prints 1503.05245, arXiv:1503.05245

Jansky, K. G. 1933, Nature, 132, 66

Kashiyama, K., Ioka, K., & Mészáros, P. 2013, ApJ, 776, L39

Katz, J. I. 2014, ApJ, 788, 34

—. 2016a, Modern Physics Letters A, 31, 1630013

—. 2016b, Modern Physics Letters A, 31, 1630013

—. 2016c, ApJ, 818, 19

Keane, E. F., Kramer, M., Lyne, A. G., Stappers, B. W., & McLaughlin, M. A. 2011, MNRAS, 415, 3065

Keane, E. F., & Petroff, E. 2015, MNRAS, 447, 2852

Keane, E. F., Stappers, B. W., Kramer, M., & Lyne, A. G. 2012, MNRAS, 425, L71

Keane, E. F., Johnston, S., Bhandari, S., et al. 2016a, Nature, 530, 453

—. 2016b, Nature, 530, 453

Keith, M. J., Jameson, A., van Straten, W., et al. 2010a, MNRAS, 409, 619

—. 2010b, MNRAS, 409, 619

Kulkarni, S. R., Ofek, E. O., & Neill, J. D. 2015, ArXiv e-prints 1511.09137, arXiv:1511.09137

Kulkarni, S. R., Ofek, E. O., Neill, J. D., Zheng, Z., & Juric, M. 2014, ApJ, 797, 70

Law, C. J., Bower, G. C., Burke-Spolaor, S., et al. 2015, ApJ, 807, 16

Li, L., Huang, Y., Zhang, Z., Li, D., & Li, B. 2016, ArXiv e-prints, arXiv:1602.06099

Loeb, A., Shvartzvald, Y., & Maoz, D. 2014, MNRAS, 439, L46

Lorimer, D. R., Bailes, M., McLaughlin, M. A., Narkevic, D. J., & Crawford, F. 2007a, Science, 318, 777

—. 2007b, Science, 318, 777

Luan, J., & Goldreich, P. 2014, ApJ, 785, L26

Lyne, A. G., & Graham-Smith, F. 1998, Pulsar astronomy

Lyubarsky, Y. 2014, MNRAS, 442, L9

Lyutikov, M. 2002, ApJ, 580, L65

Lyutikov, M., Burzawa, L., & Popov, S. B. 2016, ArXiv e-prints, arXiv:1603.02891

Macquart, J.-P., & Johnston, S. 2015, MNRAS, 451, 3278

Madau, P. 2000, ArXiv Astrophysics e-prints, astro-ph/0005106

Manchester, R. N., & Taylor, J. H. 1977, Pulsars

Maoz, D., Loeb, A., Shvartzvald, Y., et al. 2015a, MNRAS, 454, 2183

—. 2015b, ArXiv e-prints 1507.01002, arXiv:1507.01002

Masui, K., Lin, H.-H., Sievers, J., et al. 2015a, Nature, 528, 523

—. 2015b, Nature, 528, 523

Masui, K. W., & Sigurdson, K. 2015, Physical Review Letters, 115, 121301

McQuinn, M. 2014, ApJ, 780, L33

Mickaliger, M. B., McLaughlin, M. A., Lorimer, D. R., et al. 2012, ApJ, 760, 64

Milotti, E. 2002, ArXiv Physics e-prints, physics/0204033

Mottez, F., & Zarka, P. 2014, A&A, 569, A86

Narayan, R. 1992, Royal Society of London Philosophical Transactions Series A, 341, 151

Newburgh, L. B., Addison, G. E., Amiri, M., et al. 2014, in Proc. SPIE, Vol. 9145, Ground-based and Airborne Telescopes V, 91454V

Ogasaka, Y., Murakami, T., Nishimura, J., Yoshida, A., & Fenimore, E. E. 1991, ApJ, 383, L61

Oppermann, N., Connor, L., & Pen, U.-L. 2016, ArXiv e-prints, arXiv:1604.03909

Oppermann, N., Junklewitz, H., Greiner, M., et al. 2015, A&A, 575, A118

Parsons, A., PAPER, & Kilimetre Array South Africa, S. 2014, in American Astronomical Society Meeting Abstracts, Vol. 223, American Astronomical Society Meeting Abstracts #223, 404.04

Pen, U.-L., & Connor, L. 2015a, ApJ, 807, 179

—. 2015b, ApJ, 807, 179

Pen, U.-L., & Levin, Y. 2014, MNRAS, 442, 3338

Perlmutter, S., Aldering, G., Goldhaber, G., et al. 1999, ApJ, 517, 565

Peterson, J. B., Bandura, K., & Pen, U. L. 2006, ArXiv Astrophysics e-prints, astro-ph/0606104

Petroff, E., van Straten, W., Johnston, S., et al. 2014, ApJ, 789, L26

Petroff, E., Bailes, M., Barr, E. D., et al. 2015a, MNRAS, 447, 246

—. 2015b, MNRAS, 447, 246

Petroff, E., Johnston, S., Keane, E. F., et al. 2015c, MNRAS, 454, 457

Petroff, E., Keane, E. F., Barr, E. D., et al. 2015d, MNRAS, 451, 3933

Petroff, E., Barr, E. D., Jameson, A., et al. 2016, ArXiv e-prints, arXiv:1601.03547

Piro, A. L. 2016, ApJ, 824, L32

Popov, S. B., & Postnov, K. A. 2007, ArXiv e-prints, arXiv:0710.2006

Potter, T. M., Staveley-Smith, L., Reville, B., et al. 2014, ApJ, 794, 174

Press, W. H. 1978, Comments on Astrophysics, 7, 103

Rane, A., Lorimer, D. R., Bates, S. D., et al. 2015, ArXiv e-prints 1505.00834, arXiv:1505.00834

—. 2016, MNRAS, 455, 2207

Rankin, J. M., Campbell, D. B., Isaacman, R. B., & Payne, R. R. 1988, A&A, 202, 166

Ravi, V., Shannon, R. M., & Jameson, A. 2015, ApJ, 799, L5

Rickett, B. J. 1977, ARA&A, 15, 479

Riess, A. G., Filippenko, A. V., Challis, P., et al. 1998, AJ, 116, 1009

Sallmen, S., Backer, D. C., Hankins, T. H., Moffett, D., & Lundgren, S. 1999, ApJ, 517, 460

Schmidt, M. 1968a, ApJ, 151, 393

—. 1968b, ApJ, 151, 393

Scholz, P., Spitler, L. G., Hessels, J. W. T., et al. 2016a, ArXiv e-prints, arXiv:1603.08880

—. 2016b, ArXiv e-prints, arXiv:1603.08880

Shaw, J. R., Sigurdson, K., Sitwell, M., Stebbins, A., & Pen, U.-L. 2015, Phys. Rev. D, 91, 083514

Spitler, L. G., Cordes, J. M., Hessels, J. W. T., et al. 2014a, ApJ, 790, 101

—. 2014b, ApJ, 790, 101

Spitler, L. G., Scholz, P., Hessels, J. W. T., et al. 2016a, Nature, 531, 202

—. 2016b, Nature, 531, 202

Stinebring, D. R., McLaughlin, M. A., Cordes, J. M., et al. 2001, ApJ, 549, L97

Switzer, E. R., Masui, K. W., Bandura, K., et al. 2013, MNRAS, 434, L46

Taylor, M., Cinabro, D., Dilday, B., et al. 2014, ApJ, 792, 135

Tegmark, M., & Zaldarriaga, M. 2009, Phys. Rev. D, 79, 083530

Thompson, A. R., Moran, J. M., & Swenson, G. W. 1986, Interferometry and synthesis in radio astronomy

Thornton, D., Stappers, B., Bailes, M., et al. 2013a, Science, 341, 53

—. 2013b, Science, 341, 53

Tingay, S. J., Goeke, R., Bowman, J. D., et al. 2013, PASA, 30, e007

Totani, T. 2013, PASJ, 65, L12

van Haarlem, M. P., Wise, M. W., Gunst, A. W., et al. 2013, A&A, 556, A2

van Leeuwen, J. 2014, in The Third Hot-wiring the Transient Universe Workshop, ed. P. R. Wozniak, M. J. Graham, A. A. Mahabal, & R. Seaman, 79–79

Vedantham, H. K., Ravi, V., Hallinan, G., & Shannon, R. 2016, ArXiv e-prints, arXiv:1606.06795

Verheijen, M. A. W., Oosterloo, T. A., van Cappellen, W. A., et al. 2008, in American Institute of Physics Conference Series, Vol. 1035, The Evolution of Galaxies Through the Neutral Hydrogen Window, ed. R. Minchin & E. Momjian, 265–271

Voss, R. F., & Clarke, J. 1975, Nature, 258, 317

Williams, P. K. G., & Berger, E. 2016, ApJ, 821, L22

Xu, J., & Han, J. L. 2015, Research in Astronomy and Astrophysics, 15, 1629

Zanardo et al. 2014, ApJ, 796, 82

Zwicky, F. 1933, Helvetica Physica Acta, 6, 110